UNIVERSITY OF COLORADO
Boulder

Measured and Estimated pH Change and Trends Throughout the Southern Ocean, 1972-2011

A senior thesis submitted for honors in the Department of Chemistry and Biochemistry

by

Andrew Reynolds Margolin

Professor Nicole S. Lovenduski, Thesis Advisor:
Atmospheric and Oceanic Sciences

Professor Jose-Luis Jimenez, Co-Chair:
Chemistry and Biochemistry

Professor Cortlandt G. Pierpont, Co-Chair:
Chemistry and Biochemistry

April 17, 2012

Contents

List of Figures

List of Tables

Acknowledgments

We would like to thank Alex Kozyr for facilitating the CDIAC website, updating the CLIVAR database and working with us to make our pH data available on CDIAC; Ernie Lewis for assisting us with the CO2SYS Program; Claire Lo Monaco and Nicholas Metzl for assisting us with the OISO datasets; Chris Sabine for his suggestions; Rik Wanninkhof for helping us utilize the A16S data from CDIAC; Shuichi Watanabe for assisting us with JARE-34 and SR03 1994 datasets; the scientists and crews of all the hydrographic cruises. We would also like to thank Baylor Fox-Kemper for additional funding from the NSF Grant OCE 0825614; Galen McKinley for additional funding from a NASA Carbon Cycle & Ecosystems Grant; and May Panuela, the Undergraduate Research Opportunities Program (UROP), and the Professional and Academic Conference Endowment (PACE) for the opportunity to earn funding for this research as an undergraduate. This project was also partly funded by the Federal Work Study Program.

Abstract

Recent studies have shown that the Southern Ocean is experiencing changes in its carbon chemistry due to the uptake of anthropogenic CO_2 from the atmosphere, a process that lowers the pH (Sabine et al., 2004). These changes have reduced the surface carbonate concentration of the Southern Ocean by more than 10% when compared to preindustrial levels (Orr et al., 2005). Here, we have used total alkalinity, dissolved inorganic carbon, and the partial pressure of CO_2 in seawater to quantify the change of pH throughout the Southern Ocean. We calculated pH at every location where two of the parameters were measured on over sixty hydrographic cruises, and created an array of new pH data. We were able to calculate over 41,000 pH data points, resulting in a grand total of 73,477 calculated and measured pH values for our analysis. Profiles of decadal pH change from multiple repeat cruises were used to determine focus regions where pH change was most dramatic for further trend analysis. Using measurements from the 1990s to the present day we examined the vertical and spatial heterogeneity in pH trend patterns, and commented on the statistical significance of pH trends. We have determined that pH has significantly changed in the top 1 km of the water column throughout the Southern Ocean by -0.03 ± 0.03 pH units. Implications of these results will be used to assess carbon-climate model performance.

Chapter 1

Introduction

1.1 Anthropogenic CO_2 and the Global Ocean

Since the industrial revolution, humans have released approximately 244 Pg of carbon into the atmosphere as CO_2, primarily due to the burning of fossil fuels and the production of cement (Sabine et al., 2004). This anthropogenic increase in atmospheric CO_2 is warming the earth because of carbon dioxide's role as a greenhouse gas, which absorbs outgoing infrared radiation from the earth that would normally escape, creating a greenhouse effect (Sarmiento and Gruber, 2006). Some of this increased atmospheric CO_2 exchanges with the ocean and it is estimated that the ocean has absorbed approximately 30% of the total anthropogenic CO_2 emissions (Sabine et al., 2004). In order to fully understand the anthropogenic influences on global warming and climate change, it is necessary to understand how atmospheric CO_2 has been increasing due to human activity and how much of it is being absorbed by and stored in the ocean, which dampens the CO_2 induced greenhouse effect (Sarmiento and Gruber, 2006).

The CO_2 concentration in the atmosphere has not been larger than 300 ppm over the past 800 millennia (Lüthi et al., 2008), and it is evident that the recent increase in atmospheric CO_2 has been caused by anthropogenic emissions of CO_2. A continuous record of the atmospheric CO_2 concentration began in March of 1958 at the Mauna Loa Observatory in Hawaii by Dave Keeling (1960), who recorded the first atmospheric CO_2 concentration of 315.7 ± 0.1 ppm at Mauna Loa, and it has since risen to greater than 390 ppm in the past few years (Figure 1.1). Doney et al. (2009) have estimated that the atmospheric CO_2 concentration would be about 450 ppm if the ocean did not interact with the atmosphere and absorb the increasing atmospheric CO_2, which

decreases the pH of the ocean through air-sea gas exchange, also known as ocean acidification (Figure 1.1 and Section 1.2). As the CO_2 concentration in the atmosphere continues to increase because of human activity, the amount that will be absorbed by and stored in the ocean is uncertain due to various processes that could either enhance or diminish the ocean's capacity to sequester CO_2 from the atmosphere (Sarmiento and Gruber, 2006). Because of this, it is imperative that the carbon chemistry of the ocean is understood so CO_2 induced global warming and climate change can be managed successfully.

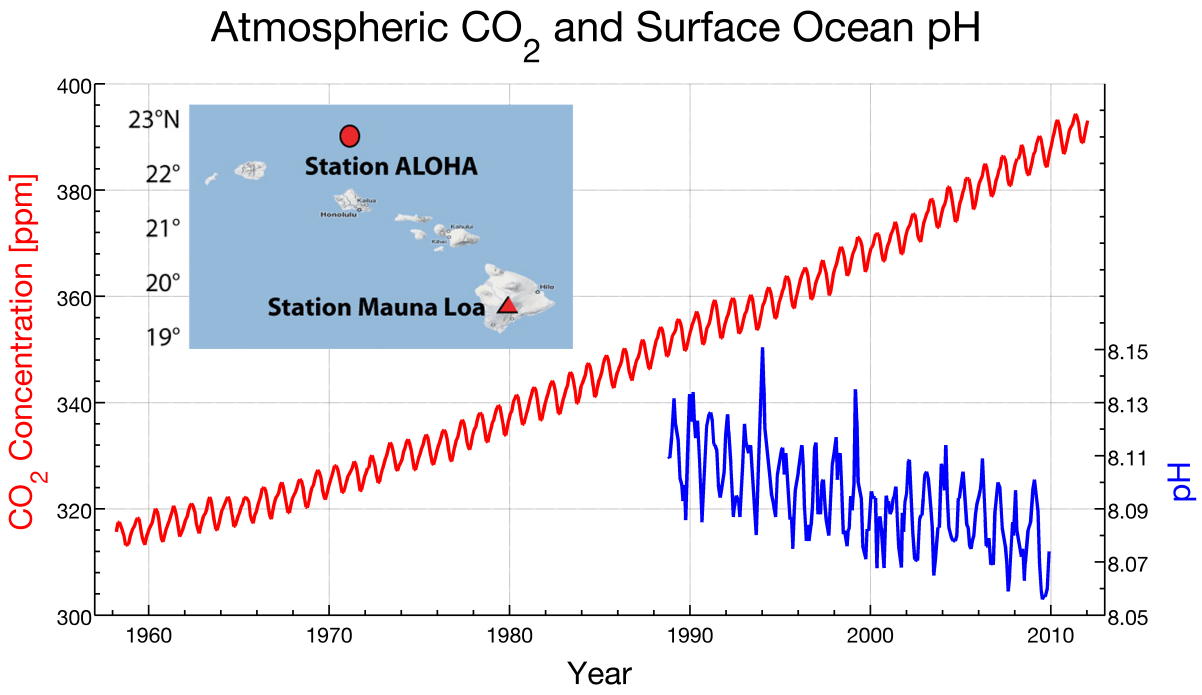

Figure 1.1: The atmospheric CO_2 concentration measured at the Mauna Loa Observatory in Hawaii since 1958 and the surface ocean pH (reported at the in situ temperature on the total hydrogen scale) measured from the Hawaii Ocean Time-Series (HOT) at Station ALOHA since 1988. The oscillating signal in CO_2 an pH represents the seasonal changes in temperature, photosynthesis and air-sea gas fluxes. Data from Keeling et al. (2012) and Dore et al. (2009), map from Doney et al. (2009).

1.2 CO_2 and Seawater

Atmospheric carbon dioxide ($CO_{2(g)}$) interacts with the ocean to become aqueous carbon dioxide ($CO_{2(aq)}$), where $CO_{2(aq)}$ undergoes a series of equilibrium reactions with water (H_2O), which

produces the hydrogen cation (H^+) in seawater (Zeebe and Wolf-Gladrow, 2001). This series of equilibria involves three other carbon species, that are formed as a result of the hydrolysis of $CO_{2(aq)}$, which are carbonic acid (H_2CO_3), bicarbonate (HCO_3^-), and carbonate (CO_3^-) and the equilibrium reactions are carried out as follows:

$$CO_{2(aq)} + H_2O \rightleftharpoons H_2CO_3 \rightleftharpoons HCO_3^- + H^+ \rightleftharpoons CO_3^{2-} + 2H^+, \tag{1.1}$$

where the carbonic acid dissociation constants govern the equilibrium between HCO_3^- and CO_3^{2-} (K_2^*), and between the two left equilibria and HCO_3^- (K_1^*) (Zeebe and Wolf-Gladrow, 2001). The reason why the leftmost equilibrium is not considered seprately with its own dissociation constant is because H_2CO_3 only composes about 0.3% of the equilibrium constituents and is often included with $CO_{2(aq)}$ and the two are referred to as CO_2 (Zeebe and Wolf-Gladrow, 2001). The importance of the carbonic acid dissociation constants, K_1^* and K_2^*, in the carbonate system will be further discussed in Section 2.3.

Consider that atmospheric CO_2 is increasing because of anthropogenic emissions as discussed in Section 1.1, which will cause more $CO_{2(g)}$ to exchange with the ocean and become incorporated into it as $CO_{2(aq)}$ and adding to the anthropogenic CO_2 content of the ocean (Figure 1.2). This increase in $CO_{2(aq)}$ will push eq. 1.1 to the right, which will result in producing more H^+ in the ocean. Increasing the H^+ concentration will lower the pH, because pH is inversely related to the $\log[H^+]$, or defined as

$$\mathrm{pH} = -\log a_{H^+}, \tag{1.2}$$

where a_{H^+} is the activity (or effective concentration) of H^+ (Zeebe and Wolf-Gladrow, 2001). It is estimated that the surface ocean pH has already decreased by 0.1 units since before the industrial revolution, and by the end of the century the surface ocean pH is expected to decrease by another 0.3-0.4 units (Orr et al., 2005; Brewer, 1997).

Now consider that the average pH of the surface ocean at the beginning of the industrial revolution was 8.2, which would make the average pH of the surface ocean 8.1 today. Also consider that by the end of this century, pH decreases by the conservative estimate of 0.3 determined by

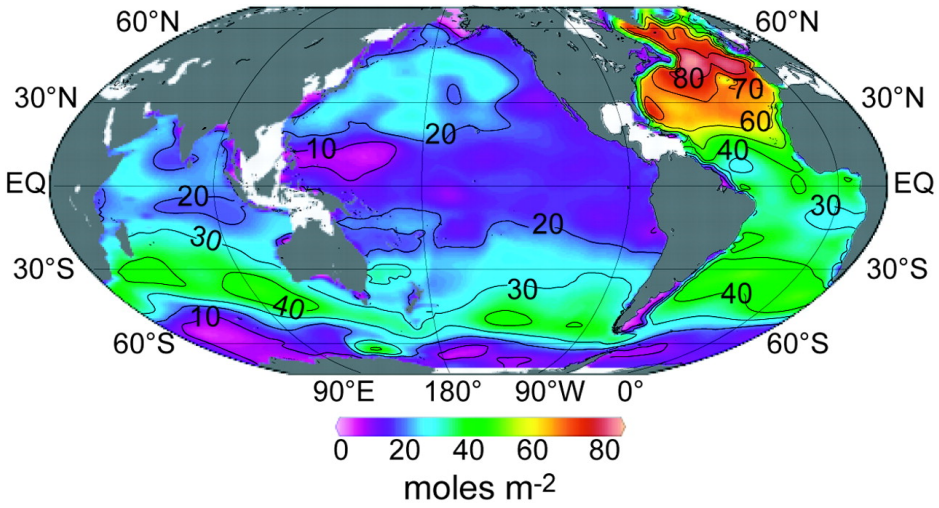

Figure 1.2: The oceanic water column inventory of anthropogenic CO_2. The largest inventories are associated with deep water formation in the North Atlantic and intermediate and mode water formation in the southern hemisphere. The total inventory of the colored region is 106 ± 17 PgC. Figure from Sabine et al. (2004).

Orr et al. (2005) and Brewer (1997) using the IS92a scenario from the Intergovernmental Panel on Climate Change (IPCC). Now let's consider how these decreases in pH will affect the three main carbon species from eq. 1.1, which are displayed in Figure 1.3. Since we are considering pH changes around 8, we will focus on CO_3^{2-} because CO_2 doesn't change much in this region of the pH scale and because HCO_3^{1-} would be approximately the same concentration change as CO_3^{2-} except in the opposite direction. If pH was at 8.2 at the beginning of the industrial revolution, the theoretical concentration of CO_3^{2-} would have been 321.5 μmol kg^{-1} (right blue dot in Figure 1.3). Assuming that the average surface ocean pH is 8.1 today, the concentration of CO_3^{2-} would be 263.4 μmol kg^{-1} (middle blue dot), which is about an 18% decrease in CO_3^{2-} concentration. Projecting to the year 2100 with the conservative estimate of a 0.3 pH decrease (left blue dot at a pH of 7.8), the concentration of CO_3^{2-} would be 140.1 μmol kg^{-1}. That's about a 56% decrease from a pH of 8.2 over ∼300 years, and most of that decrease will be happening over this century contributing to over two-thirds of the CO_3^{2-} decrease over the course of about 300 years in one-third of the time. Now let's consider what the expected biological and climatological consequences of decreasing CO_3^{2-} concentration caused by decreasing pH in the global ocean are predicted to be.

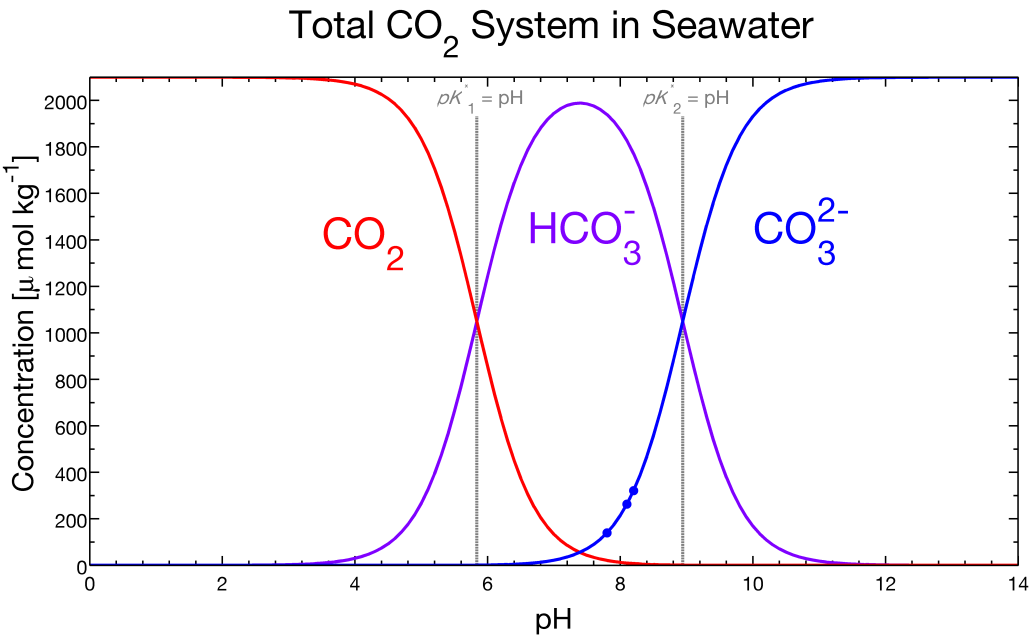

Figure 1.3: The total CO_2 system in seawater at all pH values. The "CO_2" represents $CO_{2(aq)}$ and H_2CO_3 combined and the three dots on the CO_3^- curve are at pH values of 8.2, 8.1, and 7.8. When pK_1^* and pK_2^* equal the pH value the CO_2 and HCO_3^-, and the HCO_3^- and CO_3^{2-} are respectively the same. This figure was made using the Millero et al. (2006) carbonic acid dissociation constants at 25.0°C and 36.055 psu (practical salinity units), with the total CO_2 concentration set to 2100 μmol kg^{-1} seawater, similar to Zeebe and Wolf-Gladrow (2001).

1.3 Consequences of Increased Oceanic CO_2

1.3.1 Biological Consequences

There are many organisms in the ocean that depend on the CO_3^{2-} concentration in seawater, because calcium carbonate ($CaCO_3$) is used to construct their skeletal structures and shells (Orr et al., 2005). These calcifying organisms are either composed of calcite, a stable form of $CaCO_3$, or aragonite, a metastable form of $CaCO_3$ commonly used by a variety of coral species (Kleypas et al., 1999; Orr et al., 2005). A few of these calcifying organisms that have been tested for their responses to elevated CO_2 levels are phytoplankton, which includes foraminifera and coccolithophores; mollusks, which includes pteropods, oysters, clams and squids; and arthropods, which includes copepods, crabs and krill (Fabry et al., 2008; Doney et al., 2009). Investigations were performed to determine biological responses to elevated CO_2 levels and these responses varied from organism to organism, but the most notable were that calcification and reproduction decreased,

and photosynthesis increased (Doney et al., 2009), which can be understood with the following equilibrium equation:

$$CO_2 + CaCO_3 + H_2O \rightleftharpoons 2HCO_3^- + Ca^{2+} \tag{1.3}$$

from Sarmiento and Gruber (2006). As CO_2 increases, CO_3^{2-} dissociates from $CaCO_3$ to form HCO_3^- with H_2O, which would decrease calcification resulting in a decrease in reproduction. Additionally, as CO_2 increases it can be used as a source of inorganic carbon for photosynthesis, which would increase as a result of increased CO_2 levels (Sarmiento and Gruber, 2006). However, many more laboratory and field-based studies need to be conducted before adequate predictions can be made on these responses over the course of this century (Fabry et al., 2008), although, we do have a good understanding of the solubility and dissociation of $CaCO_3$ based on its solubility product (K^*_{sp}) (Zeebe and Wolf-Gladrow, 2001).

The K^*_{sp} of $CaCO_3$ is defined as

$$K^*{}_{sp} = [Ca^{2+}]_{sat} \cdot [CO_3^{2-}]_{sat}, \tag{1.4}$$

where $[Ca^{2+}]_{sat}$ and $[CO_3^{2-}]_{sat}$ are the saturated concentrations of Ca^{2+} and CO_3^{2-} in seawater (Zeebe and Wolf-Gladrow, 2001). The relationship in eq. 1.4 becomes incredibly useful when looking at the saturation state of $CaCO_3^{2-}$ in seawater (Ω), which is defined as

$$\Omega = \frac{[Ca^{2+}]_{SW} \cdot [CO_3^{2-}]_{SW}}{K^*{}_{sp}}, \tag{1.5}$$

with the "SW" denoting concentration in seawater (Zeebe and Wolf-Gladrow, 2001). The value of Ω in eq. 1.5 is conceptually useful because when $\Omega = 1$, the saturation state of $CaCO_3$ in seawater is in equilibrium and is called the saturation horizon. If $\Omega > 1$, the seawater is supersaturated with respect to $CaCO_3$ and if $\Omega < 1$, the seawater is undersaturated and the dissociation of $CaCO_3$ occurs (Figure 1.4). Many studies have utilized Ω to determine how organisms will respond to higher CO_2 concentrations in seawater, and also to determine how the saturation horizon has changed and will change during the course of this century (Fabry et al., 2008; Feely et al., 2004; Orr et al., 2005).

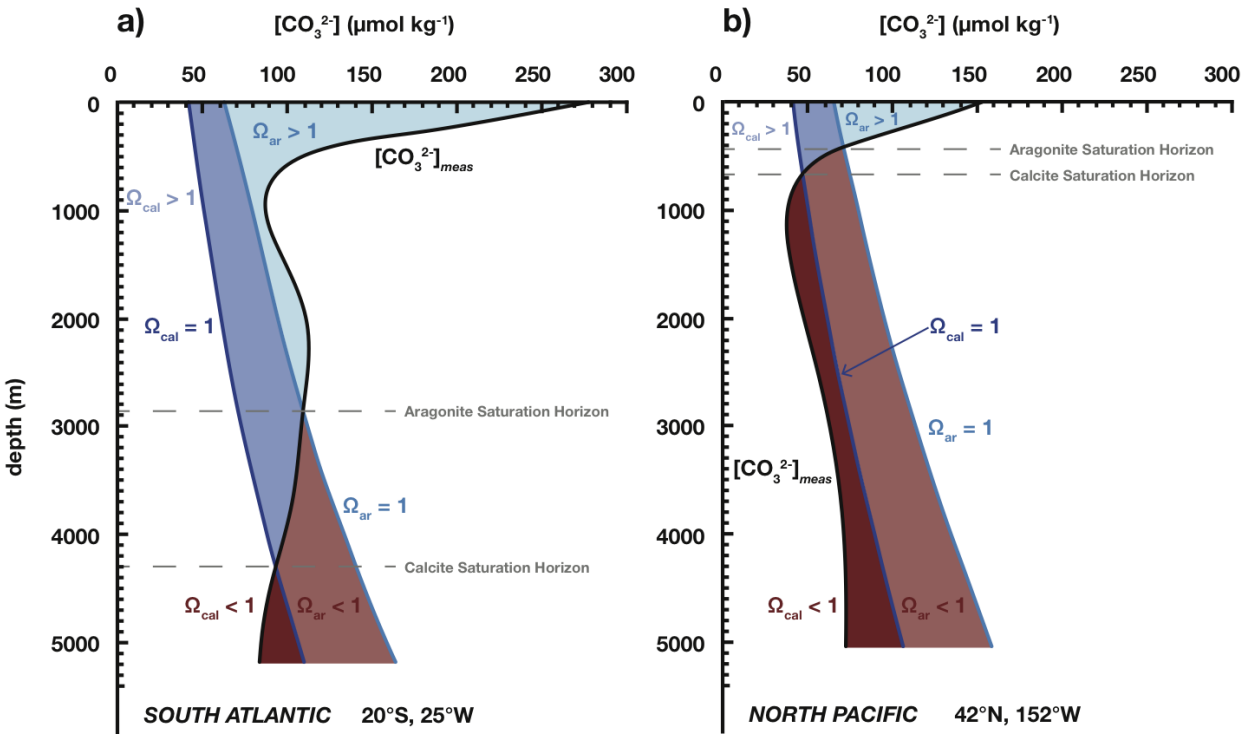

Figure 1.4: The carbonate concentration with respect to depth in the (a) South Atlantic, and (b) North Pacific. The aragonite saturation horizon is shallower than the calcite saturation horizon in both basins, illustrating aragonite's greater vulnerability. Figure adapted from Sarmiento and Gruber (2006).

Feely et al. (2004) have found that the depth of the saturation states for both calcite and aragonite (Ω_{cal} and Ω_{ar}, respectively) have shoaled in the three major ocean basins since the industrial revolution, with the saturation horizon of aragonite being more shallow than the saturation horizon of calcite, as expected from Figure 1.4. Decreases in surface Ω_{cal} and Ω_{ar} over the past two decades have already been observed from the Hawaiian Ocean Time-Series (HOT) at Station ALOHA (Figure 1.5). In order to predict how the depths of the saturation horizons for calcite and aragonite will be changing over the course of this century, Orr et al. (2005) performed a modeling study to deter-

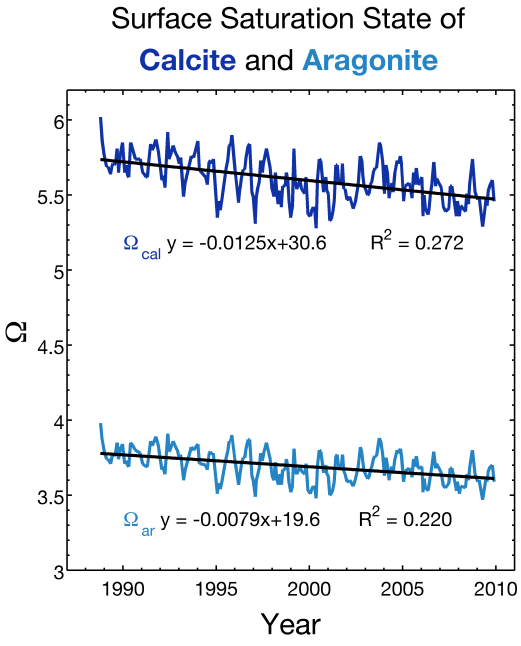

Figure 1.5: Decreases in the sea surface Ω_{cal} and Ω_{ar} from HOT at Station ALOHA. Data from Dore et al. (2009).

mine how anthropogenic ocean acidification will impact calcifying organisms based on the values of Ω_{ar} throughout the global surface ocean. Using the 'business-as-usual' scenario (IS92a scenario from the IPCC), Orr et al. (2005) found that by the year 2050 Ω_{ar} will be less than 1 in the surface water of Southern Ocean, and by 2100 this undersaturation is predicted to spread throughout the entire Southern Ocean south of 60°S (Figure 1.6). If the saturation horizon does shoal in the Southern Ocean, this will undoubtably affect a variety of trophic levels and the Southern Ocean food web dynamics (Figure 1.7) (Orr et al., 2005; Doney et al., 2009).

1.3.2 Climatological Consequenes

As discussed in Section 1.1, CO_2 in the atmosphere has increased because of anthropogenic emissions and approximately 30% of this CO_2 has been absorbed by the ocean and become $CO_{2(aq)}$. In seawater, $CO_{2(aq)}$ goes under a series of equilibrium reactions with the other carbon species that compose the total CO_2 system in seawater (eq. 1.1 and Figure 1.3), which we will refer to as dissolved inorganic carbon (DIC) if referring to it as a measured parameter rather than a system. The quantity of CO_2 in the ocean can also be determined by measuring the partial pressure of CO_2 (pCO_2), i.e., the pressure that a small volume of seawater is equilibrated with a small volume of gas, which is temperature dependent and typically recorded in μatm (Zeebe and Wolf-Gladrow, 2001). By using these two parameters (DIC and pCO_2), the buffering capacity, or the Revelle factor (R), can be determined with the following equation:

$$R = \frac{\Delta pCO_2}{pCO_2} \cdot \frac{\mathrm{DIC}}{\Delta \mathrm{DIC}}, \tag{1.6}$$

which is the fractional change in pCO_2 divided by the fractional change in DIC (Millero, 2006). The Revelle factor typically has a value between 2 and 14 with an average of about 10, which means that a 10% change in pCO_2 will only lead to approximately a 1% change in DIC (Millero, 2006). The Revelle factor is inversely proportional to the ocean's capacity to sequester CO_2 from the atmosphere, with larger Revelle factors in the cold high latitudes and smaller Revelle factors in the warm tropics (Figure 1.8) (Millero, 2006; Sabine et al., 2004). As the pCO_2 in the ocean increases (and DIC increases ~10% less than the increase in pCO_2), the ocean's capacity to absorb

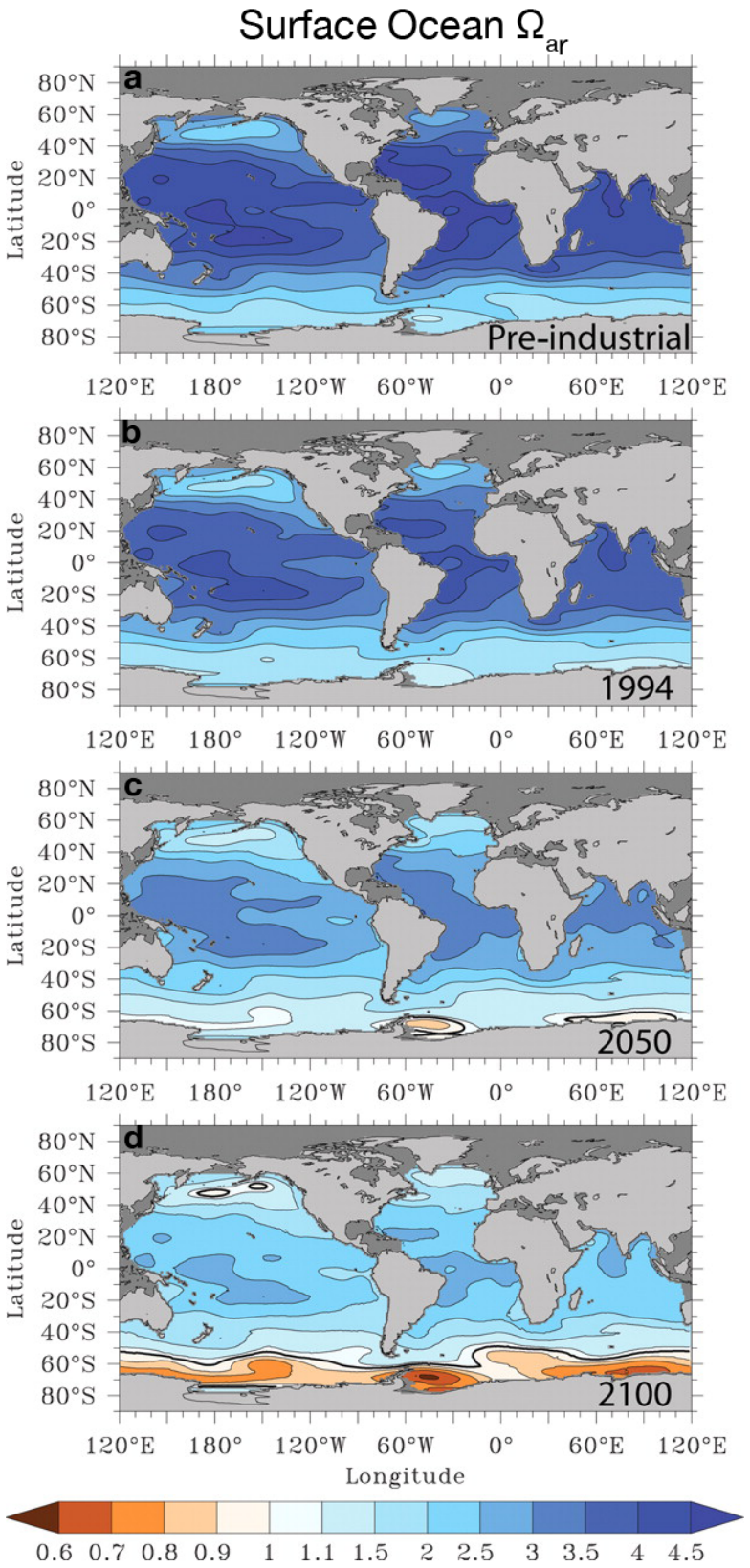

Figure 1.6: Comparison of the (a) pre-industrial, (b) 1994, (c) 2050, and (d) 2100 surface ocean aragonite saturation states determined using the 'business-as-usual' scenario, which predicts that the Southern Ocean with begin to be undersaturated with respect to aragonite by 2050. Figure from Fabry et al. (2008) using results from Orr et al. (2005).

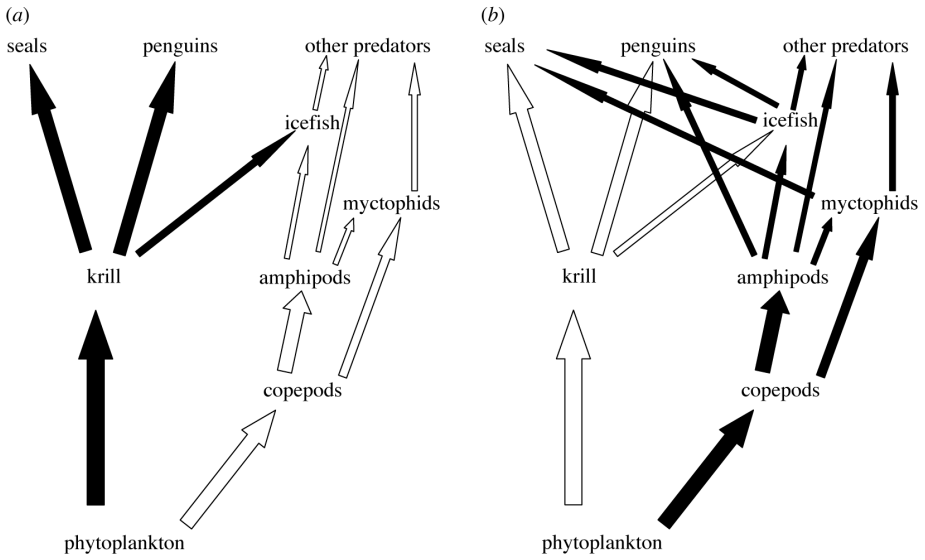

Figure 1.7: Schematic of food webs in the Scotia Sea region of the Southern Ocean (a) when krill are abundant, and (b) when krill are scarce. Notice that the four lowest trophic levels in these diagrams have been studied to determine their responses to ocean acidification, which all showed decreases in calcification and reproductivity (Fabry et al., 2008). Figure from Murphy et al. (2007).

increasing anthropogenic CO_2 from the atmosphere will decrease over time. Modeling studies have been performed that examine the coupled carbon-climate system to determine how the sink of anthropogenic CO_2 from the atmosphere into the ocean will change on decadal timescales, projecting to the end of this century (Gruber et al., 2004). It has been determined through these studies that the carbon-climate feedbacks are largely uncertain, however, they do suggest that the ocean's capacity to sequester CO_2 from the atmosphere will decrease over the course of this century, amplifying the effects of global warming (Gruber et al., 2004).

An analogous event to the projected anthropogenic CO_2 emissions from the paleo record is the Paleocene Eocene Thermal Maximum (PETM), which took place $\sim$55 million years ago when CO_2 concentrations in the ocean and atmosphere increased by an estimated 4500 giga-tons of carbon (GtC) (Doney et al., 2009; Zachos et al., 2005). The PETM coincided with global warming of at least 5°C over the course of less than ten thousand years and the increased carbon absorbed by the ocean resulted in decreases in surface ocean pH and shoaling of the calcite saturation horizon by about 2 km within 2000 years, which took over ten thousand years to recover from (Doney et al., 2009; Zachos et al., 2003). The projected anthropogenic emissions from burning the entire

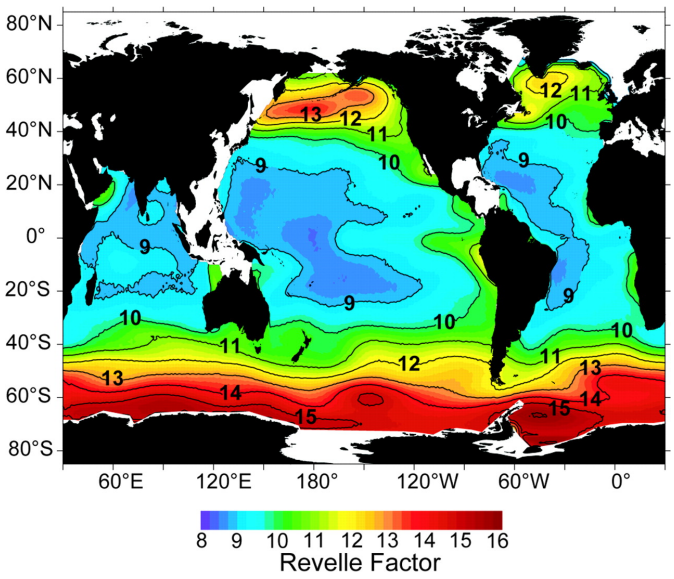

Figure 1.8: Global map of the 1994 Revelle factor averaged over the upper 50 m of the water column. Areas where the Revelle factor is low (8-11) are where the ocean is a better CO_2 sink from increasing atmospheric CO_2 concentrations than areas where the Revelle factor is high (13-16). Figure from Sabine et al. (2004).

fossil fuel reservoir (∼4500 GtC) could have similar effects on the calcite and aragonite saturation horizons throughout the water column, however, these anthropogenic emissions are estimated to take place within 300 years as opposed to millenia, which could result in far worse climatic changes due to the predicted emission time scale being shorter than oceanic overturning circulation and mixing (Zachos et al., 2005). Globally averaged surface temperatures have already increased by 0.8°C over the past century at a rate of ∼0.2°C per decade since the mid-1970s (Hansen et al., 2006). If the buffering capacity of the ocean and its ability to store CO_2 from the atmosphere are diminished, global surface temperatures will continue to rise, possibly at an accelerated rate due to the weakening of the oceanic CO_2 sink.

In addition to the decreasing buffer capacity of the ocean and the warming that results because of the ocean's limited capacity to store CO_2 from the atmosphere, fluxes of particulate organic carbon (POC) to the deep ocean will also decrease with decreasing oceanic pH (Doney et al., 2009). This is an important process that contributes to the oceanic carbon sink because POC in the surface ocean forms ballasts with $CaCO_3$, primarily produced from the decomposition of coccolithophores, which sinks to the deep ocean where this carbon is remineralized and stored

(Klaas and Archer, 2002). If the pH of the surface ocean is decreasing, causing $CaCO_3$ to dissociate at shallower depths, less POC will form ballasts and be removed from the surface ocean where it can be remineralized and emitted as CO_2 from the ocean into the atmosphere, which decreases the efficiency of the oceanic CO_2 sink (Doney et al., 2009).

1.4 The Importance of the Southern Ocean

The Southern Ocean is a unique ocean because it does not have zonal boundaries, which allows mixing between the Atlantic, Indian and Pacific Oceans by the eastward Antarctic Circumpolar Current (ACC) that circulates around Antarctica (Talley et al., 2011). In addition to the unique zonal circulation, the Southern Ocean also contributes multiple water masses to the meridional overturning circulation (MOC), which circulates water masses throughout the global ocean (Talley et al., 2011). The water masses that circulate through the Southern Ocean are Antarctic Bottom Water (AABW), Upper and Lower Circumpolar Deepwater (UCDW and LCDW, respectively), North Atlantic Deep Water (NADW), Antarctic Intermediate Water (AAIW), and Subantarctic Mode Water (SAMW) (Speer et al., 2000). These water masses and their circulation patterns form what is called the Deacon cell, which is driven by the interactions between cold, dense layers and warm, low-density layers of water (Figure 1.9) (Speer et al., 2000). Water masses that form in the Southern Ocean are AABW, on the Antarctic continental margin, and AAIW and SAMW formed north of the Polar Front (PF), whereas the other water masses are either ventilated or mixed in the Southern Ocean (Speer et al., 2000).

The vertical motion of water caused by the Deacon cell and MOC, creates areas in the Southern Ocean where naturally and anthropogenically produced CO_2 exchanges between the atmosphere and the ocean. However, since the last time the ventilating water masses were at the surface ocean was before the industrial revolution (Sarmiento and Gruber, 2006), only natural CO_2 is outgassed from the ocean, while natural *and* anthropogenic CO_2 are being incorporated into the ocean (Figure 1.9). Because of this, we are primarily interested in areas where CO_2 is being incorporated into the ocean by AAIW and SAMW formation, and at the Antarctic continental margin where AABW is formed. We are interested in these areas because they are where the pH of

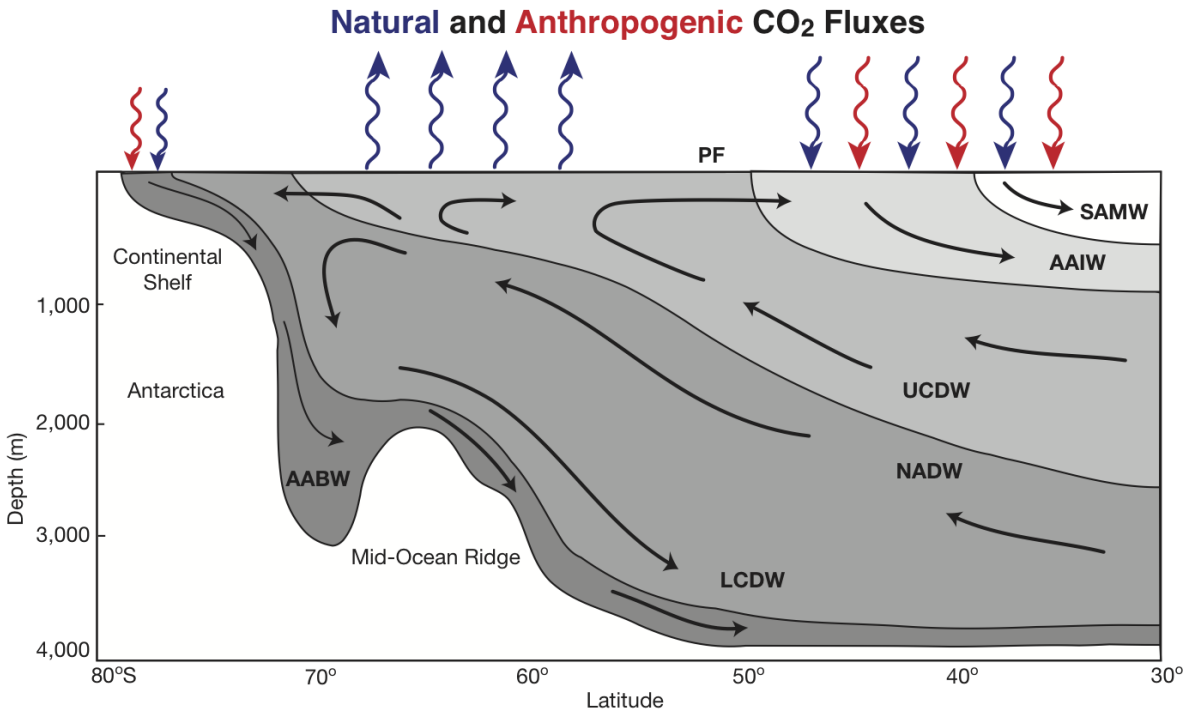

Figure 1.9: The MOC in the Southern Ocean and the various water masses that compose the Deacon cell. The black arrows represent flow of the corresponding water masses, while the wavy arrows represent locations where CO_2 gas exchange takes place between the atmosphere and the ocean. Adapted from Speer et al. (2000).

the ocean could be significantly decreasing due to the air-sea gas exchange between the atmosphere and ocean, and the resulting incorporation of anthropogenic CO_2 into the interior of the ocean.

There are two major locations in the global ocean where interior water masses are formed at the surface ocean; one being in the North Atlantic were NADW is formed, and the other being the Southern Ocean where AABW, AAIW, and SAMW are formed (Talley et al., 2011). The formation of NADW is estimated to incorporate approximately 7 Pg of anthropogenic carbon into the interior ocean, while the formation of the combined AAIW and SAMW is estimated to incorporate approximately 20 Pg of anthropogenic carbon into the interior ocean (Sabine et al., 2004). The reason for the much larger amount of anthropogenic carbon entering the interior of the ocean in the southern hemisphere is because the formation of AAIW and SAMW is not limited to one basin, in contrast with NADW, which is (Figure 1.2). Even though the anthropogenic carbon signatures of AAIW and SAMW are not as concentrated as the NADW signature, since they both have complete zonal coverage between 30°S and 50°S, their contributions as anthropogenic carbon

sinks from the atmosphere are far more significant than the contributions of NADW (Sabine et al., 2004). It is also important to note that the northern hemisphere is more frequently measured than the southern hemisphere, e.g., every month out of the year surface water pCO_2 has been measured in the North Atlantic and North Pacific in contrast with the Southern Ocean where the only area with 12-month surface pCO_2 data is the Drake Passage (Figure 1.10) (Takahashi et al., 2009). One of the reasons for the seasonally biased sampling of the Southern Ocean when compared to the North Atlantic and North Pacific is because of the large variability in sea ice extent, which leaves most of Southern Ocean south of 60°S covered in ice and inaccessible by ship during the austral winter (Figure 1.11).

In order to understand how the carbon chemistry of the Southern Ocean will be changing due to anthropogenic CO_2 emissions and changes in atmospheric circulation patterns, modeling studies have been performed that investigate how the CO_2 fluxes throughout the Southern Ocean and how the surface ocean Ω_{ar} will be different by the end of this century (Lovenduski and Ito,

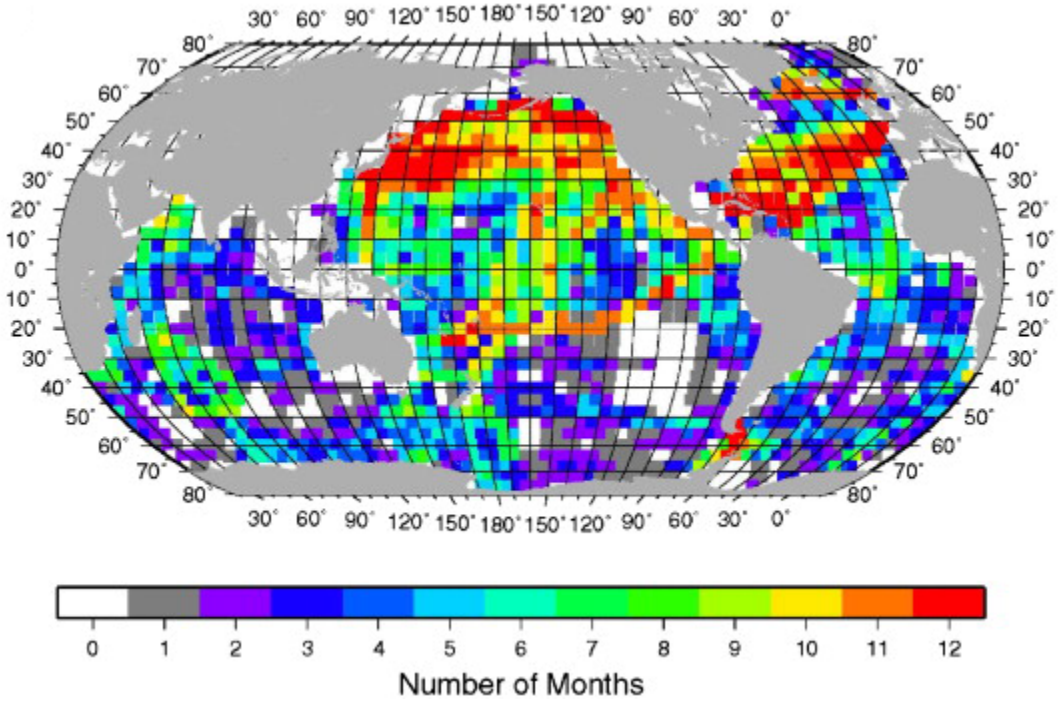

Figure 1.10: Number of months where surface water pCO_2 has been measured since the early 1970s. The colored areas represents 4°×5° grid cells where pCO_2 has been measured at least once during the respective month. Figure from Takahashi et al. (2009).

2009; Orr et al., 2005). Both studies concluded that the Southern Ocean's role as a CO_2 sink from the atmosphere remains uncertain over the course of this century due to the various atmospheric CO_2 concentrations projected and the unknown changes in atmospheric and oceanic circulation. A comparison of the changes in the surface ocean Ω_{ar} over time can be seen in Figure 1.6.

In this work, we examined decadal pH change along three repeat hydrographic transects in each of the three major ocean basins to determine pH trends throughout the water column at various latitudes throughout the southern hemisphere. A majority of the pH values we used were calculated for this study, creating over 41,000 calculated pH data points using other measured parameters sampled throughout the Southern Ocean ranging from the earliest measurements in 1972, to the most recent in 2011. In addition to the calculated pH values produced, we have normalized all measured and calculated pH values to the same temperature and pH scale so values can be directly compared for determining pH changes throughout the southern hemisphere over the course of the past four decades. The over 41,000 pH values calculated from this study are being prepared to be made publically available online to contribute to the broader understanding of the changing carbon chemistry throughout the Southern Ocean.

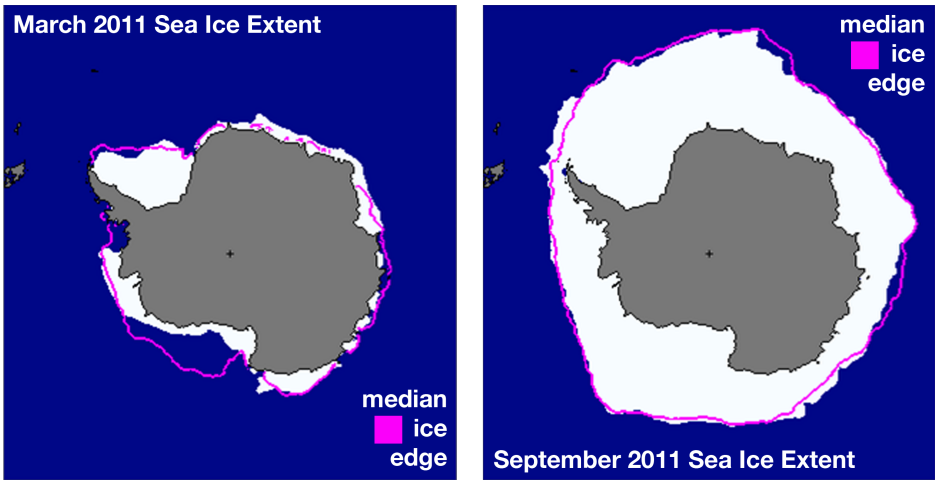

Figure 1.11: Seasonal variations in the Southern Ocean sea ice extent. The total sea ice extent covered an area of 3.6×10^6 km^2 in March 2011 and an area of 18.9×10^6 km^2 in September 2011, which is over five times the areal coverage in March. Figure from the National Snow and Ice Data Center, Boulder, CO.

Chapter 2

Determining pH using the Carbonate System in Seawater

2.1 Introduction

The overarching goal for this project was to quantify and understand past changes in Southern Ocean pH. In order to achieve this goal, we needed to calculate pH values based on other previously measured parameters, such as DIC and pCO_2 that were introduced in Section 1.3.2. Using these parameters we were able to calculate pH throughout the Southern Ocean and significantly improve the southern hemisphere pH coverage using our calculated values. Here, we introduce the hydrographic datasets where data were obtained and discuss our motivations behind improving the southern hemisphere pH dataset with calculated pH values. We will also discuss the calculations that were performed, using a program called CO_2 System Calculations (CO2SYS), in order to calculate pH values where pH was not previously measured (Lewis and Wallace, 1998). We will also discuss how this calculation was optimized in order to calculate pH with the highest accuracy by comparing these calculated pH values with measured pH.

2.2 Data Sources and Motivation

They earliest hydrographic data that we used for this study was from the Atlantic Ocean Geochemical Ocean Section Study (GEOSECS), which took place during the 1970s (Sarmiento and Gruber, 2006). About two decades after the GEOSECS program, the World Ocean Circulation

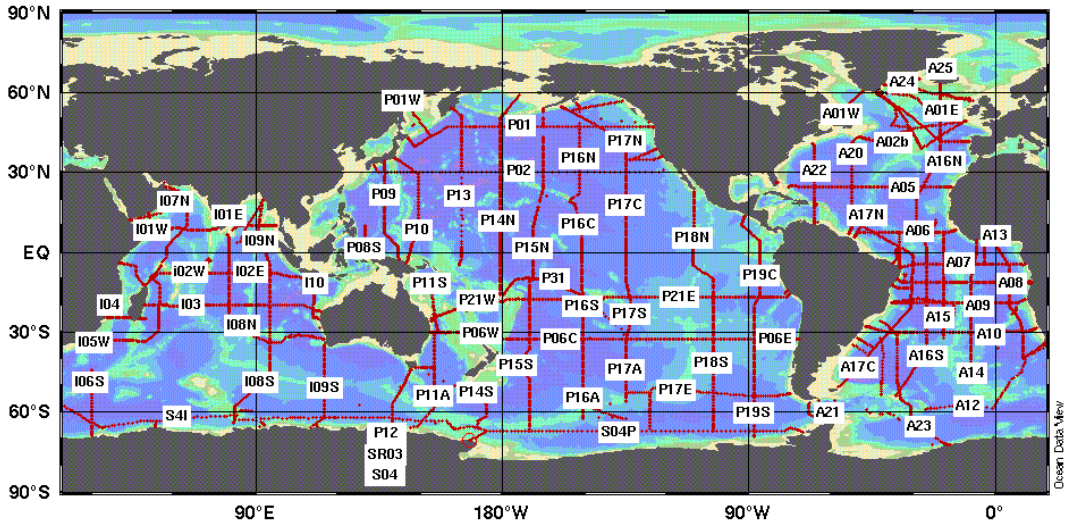

Figure 2.1: Available Hydrographic Data from WOCE. The red dots represent the approximate hydrographic sampling coverage of the oceans. Figure from Kozyr (2011).

Experiment (WOCE) (Figure 2.1) began in the 1990s and lasted for approximately one decade, which was replaced by the Climate Variability and Predictability (CLIVAR) Global Ocean Carbon and Repeat Hydrography Program in the 2000s (Sarmiento and Gruber, 2006; Kozyr, 2011). The majority of the data used for this study came from the Carbon Dioxide Information and Analysis Center (CDIAC), through various programs such as WOCE and the international CLIVAR repeat program, which we used as primary data sources (Kozyr, 2011). Other sources from CDIAC were used to obtain data from cruises outside the scope of WOCE and the CLIVAR repeat program, such as the Global Ocean Data Analysis Project (GLODAP), and Carbon in the Atlantic Ocean Data Synthesis Project, (CARINA) (Kozyr, 2011). There were a few hydrographic sections that were not obtained through CDIAC, which were obtained through the CLIVAR and Carbon Hydrographic Data Office (CCHDO) (Swift et al., 2012).

Ship-based measurements performed during these programs were carried out using a CTD-rosette to sample throughout the water column. A CTD is a sensor that measures the conductivity (C) of seawater to determine salinity, measures the temperature (T), and measures the pressure to determine depth (D). This CTD sensor is attached to a rosette containing 24 Niskin bottles, which can be triggered to close at specified depths to collect water so various chemical properties of seawater can be measured in the laboratory. Two out of the 24 bottles are typically used to

obtain repeat samples for precision analysis, so 24 measurements are taken at 22 unique depths with every CTD-rosette cast. The average depth of the ocean is about 4 km (Talley et al., 2011), so the vertical spacing between collected samples is typically about 25 m near the surface up to hundreds of meters at depth and horizontal sampling stations range from about 0.5° to 1° (55.5 to 111 km).

The motivation for this study was to improve the pH data available because a majority of the cruise transects represented in Figure 2.1 did not measure pH, and when the transects were later repeated in the 2000s through CLIVAR, only a small portion of them measured pH (Figure 2.2). During the WOCE program, pH was extensively under-sampled and it continues to be under-sampled in the repeat program, especially in the Southern Ocean. Because of the important role of the Southern Ocean as an anthropogenic carbon sink and the consequences of the oceanic carbon sink illustrated by Orr et al. (2005) and Sabine et al. (2004), we decided to calculate pH using carbon parameters that were measured to improve the Southern Ocean pH coverage with our calculated pH values. Using this calculated pH dataset we were able to determine how pH in the Southern Ocean has changed since the 1990s and we plan to look at regional trends throughout the Southern Ocean since the 1970s, during the GEOSECS program. Additionally, the pH data that we have produced will be made available online for public use.

2.3 The Carbonate System in Seawater

The carbonate system in seawater is important to the study of chemical oceanography and environmental sciences because it controls the acidity of seawater and is influenced by the air-sea gas exchange of CO_2 , and both topics are at the forefront of present climate change (Emerson and Hedges, 2008). There are four components that compose the carbonate system in seawater, and those are DIC, which was introduced in Section 1.3.2; total alkalinity (TA); pH; and either the partial pressure or fugacity of CO_2 (pCO_2 or fCO_2, respectively) (Lewis and Wallace, 1998). The difference between pCO_2 and fCO_2 is small and for the purpose of this paper we will refer to both

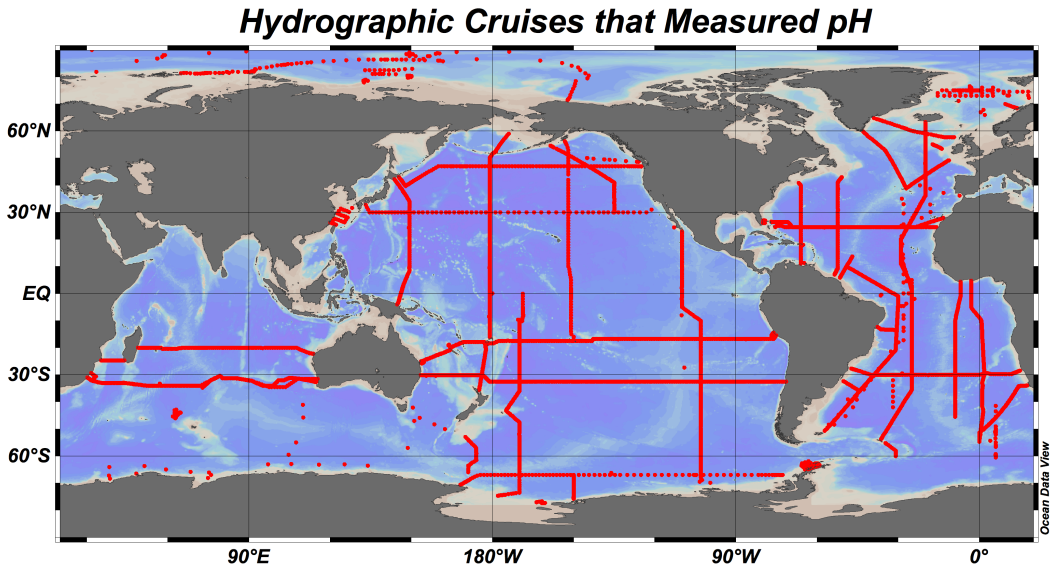

Figure 2.2: Hydrographic cruises that measured pH during WOCE and CLIVAR.

as pCO_2 (Emerson and Hedges, 2008), although, we did treat pCO_2 and fCO_2 differently for the pH calculations. DIC and TA are defined as:

$$\mathrm{DIC} = [H_2CO_3] + [HCO_3^-] + [CO_3^{2-}] + [CO_{2(aq)}] \tag{2.1}$$

and

$$\begin{aligned}\mathrm{TA} = {} & [HCO_3^-] + 2[CO_3^{2-}] + [B(OH)_4^-] + [OH^-] + [HPO_4^{2-}] + 2[PO_4^{3-}] + [SiO(OH)_3] \\ & + [HS] + 2[S] + [NH_3] - [H^+] - [HSO_4^-] - [HF] - [H_3PO_4],\end{aligned} \tag{2.2}$$

according to Dickson (1981), where both have units of μmol kg^{-1} seawater, where 1 kg of seawater $\approx$ 1 L of seawater. However, for our purposes calculating pH we are not including [HS], 2[S] and [NH_3] in the definition of TA according to Lewis and Wallace (1998). pCO_2 is defined as the partial pressure of CO_2 when seawater is equilibrated with a small volume of gas measured in units of μatm (Section 1.3.2). Two out of three of these chemical parameters, along with pH, can be used to calculate the other two using the carbonic dissociation constants, K_1^* and K_2^* (Section 1.2).

Finally, the definition of pH is:

$$\mathrm{pH} = -\log_{10}(\mathrm{a_H}), \tag{2.3}$$

where $\mathrm{a_H}$ is the hydrogen ion activity or an effective hydrogen concentration (Zeebe and Wolf-Gladrow, 2001). Since there are multiple pH scales that are used and pH (along with $p\mathrm{CO_2}$) is sensitive to temperature, one of these scales and temperatures will need to be used in order to compare pH values. For our use determining pH changes and trends all pH values, whether calculated or measured, were converted to the seawater scale ($\mathrm{pH_{SWS}}$) at 25°C so their values could be compaired and pH change could be determined. The definition of the hydrogen ion activity on the seawater scale is:

$$\mathrm{a_{H_{SWS}}} = f_{\mathrm{H}} \cdot [\mathrm{H^+_{SWS}}], \tag{2.4}$$

where f_{H} is the activity coefficient of the hydrogen ion and $[\mathrm{H^+_{SWS}}]$ defined as:

$$[\mathrm{H^+_{SWS}}] = [\mathrm{H^+}] + [\mathrm{HSO_4^-}] + [\mathrm{HF}] \tag{2.5}$$

(Lewis and Wallace, 1998; Millero et al., 2006).

As previously mentioned, pH and $p\mathrm{CO_2}$ are sensitive to temperature, whereas DIC and TA are not. Because of this sensitivity, pH and $p\mathrm{CO_2}$ are considered non-conservative properties of seawater, i.e., if the temperature changes the number of hydrogen cations and the amount of $\mathrm{CO_{2(g)}}$ in seawater will change. Conversely, because the measurements of DIC and TA do not depend on temperature, these two chemical parameters of seawater are considered to be conservative, or non-reactive (Zeebe and Wolf-Gladrow, 2001). Since DIC and TA are conservative parameters in the carbonate system in seawater, they are more frequently measured on hydrographic cruises than pH or $p\mathrm{CO_2}$. That is why a number of the cruises in Figure 2.1 did not measure pH, however, during most of those cruises DIC and TA were measured. It is also important to note that $\mathrm{CO_3^{2-}}$ is also a non-conservative parameter like pH and $p\mathrm{CO_2}$, which is why $\mathrm{CO_3^{2-}}$ is also not measured frequently, but these three non-conservative parameters can be calculated if DIC and TA are measured (Lewis and Wallace, 1998).

2.4 Optimizing the pH Calculation and Normalizing Data

To determine the accuracy of the pH values calculated using CO2SYS, forty-four cruises that measured pH along with two other inorganic carbon parameters (DIC, TA and pCO_2) were used to validate the CO2SYS calculation. Since these forty-four cruises reported pH on various pH scales and at different temperatures, measured pH values were not converted to a standard temperature or scale so no conversion error was introduced to the pH calculation for determining its accuracy. Calculated pH values were determined using eight out of ten carbonic acid dissociation constant pairs, K_1^* and K_2^* previously introduced in Section 1.2, and the Dickson (1990) sulfate dissociation constant ($K^*_{SO_4}$). The eight carbonic acid dissociation constants pairs that were used for this analysis were Roy et al. (1993), Goyet and Poisson (1989), Hansson (1973b,a) refit by Dickson and Millero (1987), Mehrbach et al. (1973) refit by Dickson and Millero (1987), Hansson (1973b,a) and Mehrbach et al. (1973) refit by Dickson and Millero (1987), GEOSECS (Takahashi et al., 1982), Millero et al. (2006), and Lueker et al. (2000). The only two carbonic acid dissociation constant pairs from CO2SYS that we did not use were Peng et al. (1987) and Millero (1979) because these dissociation constants were reported to only works for pure water.

Another factor in the calculation that we considered was that salinity was frequently measured using two techniques. Salinity is always measured in situ using the CTD sensor and commonly a second time in the laboratory from the Niskin bottle samples. All of the CTD salinity measurements have a WOCE CTD flag corresponding to the quality of the measurement. For our calculations, the only flags that were accepted were 2 (acceptable measurement) and 6 (interpolated over greater than 2 dbar level) (Swift et al., 2001). Because the pH calculation is not incredibly sensitive to the accuracy of salinity measurements and because 2 dbar is approximately equal to only 2 m, we found 6 to be an acceptable flag for our purposes as well. Salinity that was measured in a laboratory from a bottle was assigned different flags, which are the WOCE bottle sample flags (Swift et al., 2001). Again, the only flags that were accepted were 2 (acceptable measurement) and 6 (mean of replicate measurements) (Swift et al., 2001).

Other parameters that were used for the CO2SYS calculation besides salinity, TA, DIC, pCO_2, and pH were silicate, and phosphate and all had the same WOCE bottle sample flags as

salinity corresponding to the quality of the reported measurement. If there were any flags not equal to 2 or 6 the data point from that measurement was not used to calculate pH. Since salinity was measured using two different techniques we took used the bottle measurements over the CTD measurements due to the measurement environment. If however, bottle salinity was not measured or discarded because of a flag and it was measured by the CTD with a 2 or 6 quality flag, the CTD salinity measurement was used. Similarly, if silicate or phosphate were not measured or discarded because of a flag their values were set to 0 μmol kg^{-1}. Control experiments were carried out when pH was calculated using measured silicate and phosphate values, and calculated again with those concentrations were set to 0 μmol kg^{-1} and the difference between the two pH calculation methods was on the order of 10^{-6} pH units, i.e., beyond our limit of detection. The error that we are reporting for calculated pH (pH$_{calc}$) values is larger than this discrepancy and we have determined that it is negligible.

Once pH was calculated for all forty-four cruises the root-mean-square error (RMSE) of pH$_{calc}$ compared to measured pH (pH$_{meas}$), i.e.,

$$\mathrm{RMSE}(\mathrm{pH}_{calc}) = \sqrt{\frac{\sum_{i=0}^{n}(\mathrm{pH}_{meas} - \mathrm{pH}_{calc})^2}{n}} = \sigma_{calc} \tag{2.6}$$

was calculated for the individual cruises to determine if there were any outliers prior to taking the RMSE of all forty-four cruises to determine the overall accuracy of CO2SYS pH calculation (Figure 2.3 and Table 2.1). The A16S 1991 pH calculation was an order of magnitude higher than most other cruises, likely because the computer that was supposed to run the titrator on the A16S 1991 cruise broke and titrations were done manually (Wanninkhof and Hendee, 1991). This is most likely the reason for the larger RMSE for the A16S 1991 pH calculation so A16S 1991 was excluded from the CO2SYS accuracy determination. There were a few other cruises that had RMSE's similar to A16S 1991, so Dixon's Q-test was used to validate their exclusion from the CO2SYS accuracy determination with a confidence level better than 95% (Rorabacher, 1991). For a list of individual cruise CO2SYS pH calculation RMSE's and dissociation constants see Section B.1, and for CO2SYS pH calculation RMSE's for all cruises see Figure 2.3 and Table 2.1.

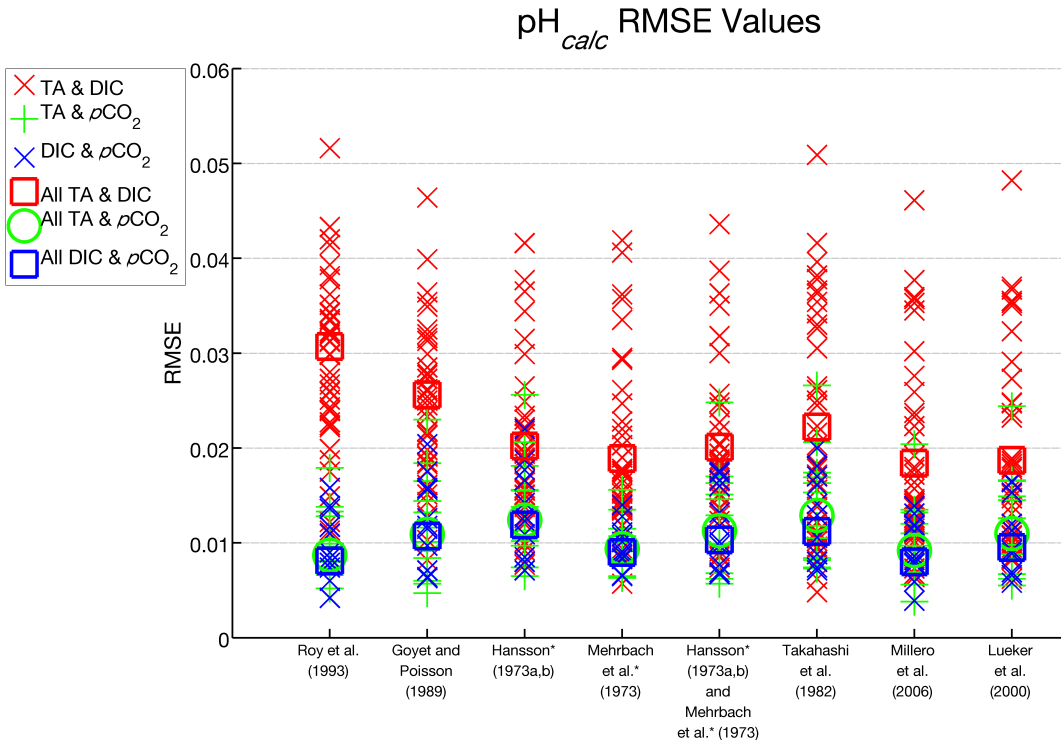

Figure 2.3: RMSE of CO2SYS pH calculations. The RMSE values for individual cruises that measured pH along with two other inogranic carbon parameters are denoted with $\times$ and $+$ symbols. The RMSE values for all values compiled from all cruises are denoted with $\square$ and $\bigcirc$ symbols. The number of cruises for each total RMSE values are $n = 40$ for TA and DIC, $n = 12$ for TA and pCO_2, and $n = 11$ for DIC and pCO_2 values. *Refit by Dickson and Millero (1987).

The accuracy determined for pH_{calc} values reported in Table 2.1 were used with the repeat bottle sample precision values (discussed in Section 2.2) from the forty-one cruises that measured inorganic carbon parameters that accurately produced pH_{calc} values using CO2SYS. The mean of the precision estimates from the forty-one cruises was propagated with the pH_{calc} to determine the overall pH_{calc} error, e.g.,

$$\sigma(\mathrm{pH}_{calc}) = \sqrt{(\frac{1}{n}\sum_{i=0}^{n}\sigma_{rep})^2 + {\sigma_{calc}}^2}, \tag{2.7}$$

where σ_{calc} is the accuracy estimate from eq. 2.6, σ_{rep} is the precision estimate from repeat measurements and n is the number of cruises. This calculation was performed for each of the three parameter combinations used to calculate pH with CO2SYS and the pH_{calc} accuracy, pH_{meas} precision and propagated pH_{calc} error are reported in Table 2.2.

The σ_{calc} values were used to assign calculation flags for every pH calculation, based on

RMSE for all Cruises and Dissociation Constants						
CO2SYS parameters	DIC & TA	DIC & TA	TA & pCO_2	TA & pCO_2	DIC & pCO_2	DIC & pCO_2
Number of cruises	43	40	14	12	13	11
Dissociation constants						
Roy et al. (1993)	0.0368	0.0307	0.0230	0.0087	0.0234	0.0081
Goyet and Poisson (1989)	0.0326	0.0256	0.0248	0.0109	0.0253	0.0107
Hansson (1973b,a)*	0.0284	0.0202	0.0259	0.0124	0.0261	0.0119
Mehrbach et al. (1973)*	0.0274	0.0189	0.0220	0.0094	0.0220	0.0090
Hansson (1973b,a) and Mehrbach et al. (1973)*	0.0284	0.0201	0.0246	0.0113	0.0247	0.0103
GEOSECS	0.0291	0.0222	0.0253	0.0129	0.0247	0.0112
Millero et al. (2006)	0.0269	0.0184	0.0228	0.0092	0.0226	0.0080
Lueker et al. (2000)	0.0269	0.0187	0.0245	0.0110	0.0241	0.0095

Table 2.1: RMSE for all all forty-four cruises that measured either DIC, TA, or pCO_2 produced using the associated dissociation constants before and after the Q-test exclusions. *Refit by Dickson and Millero (1987), and GEOSECS is from (Takahashi et al., 1982). We found that Millero et al. (2006) produced the most accurate pH_{calc}, with the exception of Roy et al. (1993) for TA and pCO_2. However, since there is no significant difference between the RMSE from Roy et al. (1993) and Millero et al. (2006) if they are rounded to one significant figure, so Millero et al. (2006) dissociation constants were determined to be best for calculating pH.

the values from Table 2.2 and Section B.1. We assumed that there was no error associated with converting pH from one scale to another and our flag assignments and associated error can be seen in Table 2.3. Calculated pH values were used based on their flag and associated calculation error, e.g., if pH was calculated throughout the cruise transect with flags 1, 2 and 4, all of the pH_{calc} values associated with flag 1 were used. If flag 2 pH_{calc} values existed where there were no flag 1 pH_{calc} values, pH_{calc} with flag 2 filled in the blanks, and again, flag 4 pH_{calc} values filled in the flag 1 and 2 pH_{calc} gaps. Since the calculated pH value depended on the measurement of two carbon parameters along with salinity measurements, the spatial coverage of pH using calculated values is not as robust when compared to the coverage of measured pH, however, calculated pH values do represent pH accurately (Figure 2.4).

Accuracy, Precision, and Error Associated with pH_{calc}				
Parameter Combinations	σ_{calc}	σ_{rep}	$\sigma(pH_{calc})$	σ_{sig}
DIC & TA	0.0184	0.0038	0.0188	0.02
TA & pCO_2	0.0092	0.0038	0.0100	0.01
DIC & pCO_2	0.0080	0.0038	0.0089	0.009

Table 2.2: The accuracy of the CO2SYS calculation (σ_{calc}), the precision of the bottle measurements (σ_{rep}), the overall error of pH_{calc} values ($\sigma(pH_{calc})$), and the overall error of pH_{calc} values rounded to one significant figure (σ_{sig}).

Calculation Flags and the Associated Error		
Calculation Flag	CO2SYS Parameters	Associated Error
0	pH_{SWS} at 25°C	0
1	pH and pCO_2	assumed 0
2	DIC and pH	assumed 0
3	TA and pH	assumed 0
4	DIC and pCO_2	0.009
5	TA and pCO_2	0.01
6	TA and DIC	0.02
7	$\sim pH_{SWS}$ at 25°C	0.1
8	$\sim$pH and pCO_2	0.1
9	DIC and $\sim$pH	0.1
10	TA and $\sim$pH	0.1

Table 2.3: pH calculation flags and the associated error. The associated error for pH conversions was assumed to be zero because pH was not measured on two scales, one being the seawater scale to check for accuracy. "$\sim$" symbolizes questionable pH measurements due to no flags assignment, such as the one from A16S 1991. Questionable pH values with errors on the order of 0.1 were not used for our analysis.

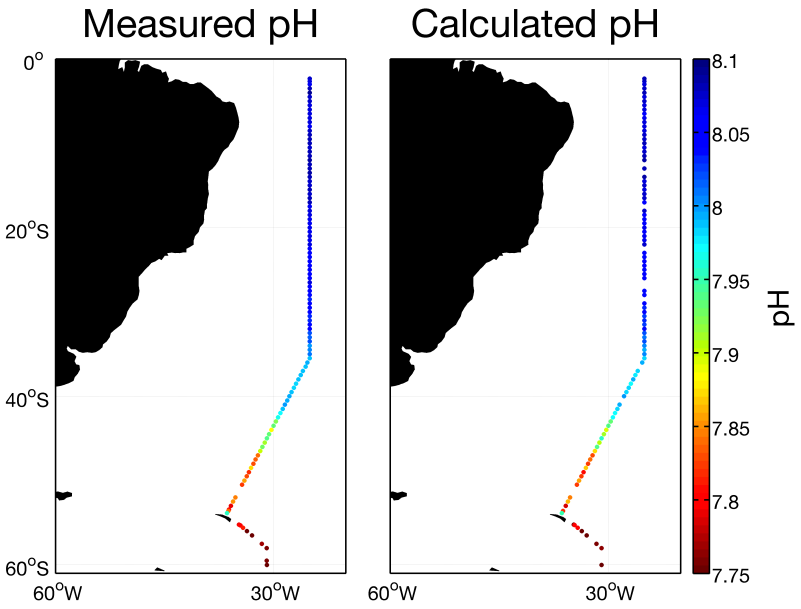

Figure 2.4: Measured (a) and calculated (b) pH in the top 30 m along the A16S transect in the South Atlantic. This demonstrates the utility of being able to calculate pH where pH values do not exist, however, it also illustrates the shortcomings of calculated pH by the calculated data being more sparse.

2.5 Results and Discussion

Based on the methods employed to determine the accuracy of the CO2SYS calculation along with the precision estimates from repeat bottle measurements, errors associated with calculated pH values were determined. These pH_{calc} errors range from better than $\pm$ 0.009 pH units to $\pm$ 0.02, depending on the two parameters measured and used to calculate pH. There was an assumption made that larger pH_{calc} RMSE's could be excluded from the CO2SYS error determination because the calculated pH values were significantly different than the measured pH values based on Dixon's Q-test (Rorabacher, 1991), which we determined to be associated with either measurement or documentation errors as opposed to calculation errors. We determined that the most accurate carbonic acid dissociation constants are the Millero et al. (2006) dissociation constants, which we will use for our analysis of pH change in the Southern Ocean. Using these dissociation constants we are able to calculate pH values throughout the water column that are within $\pm$ 0.02 pH values of measured pH values (Figures 2.5 and 2.6).

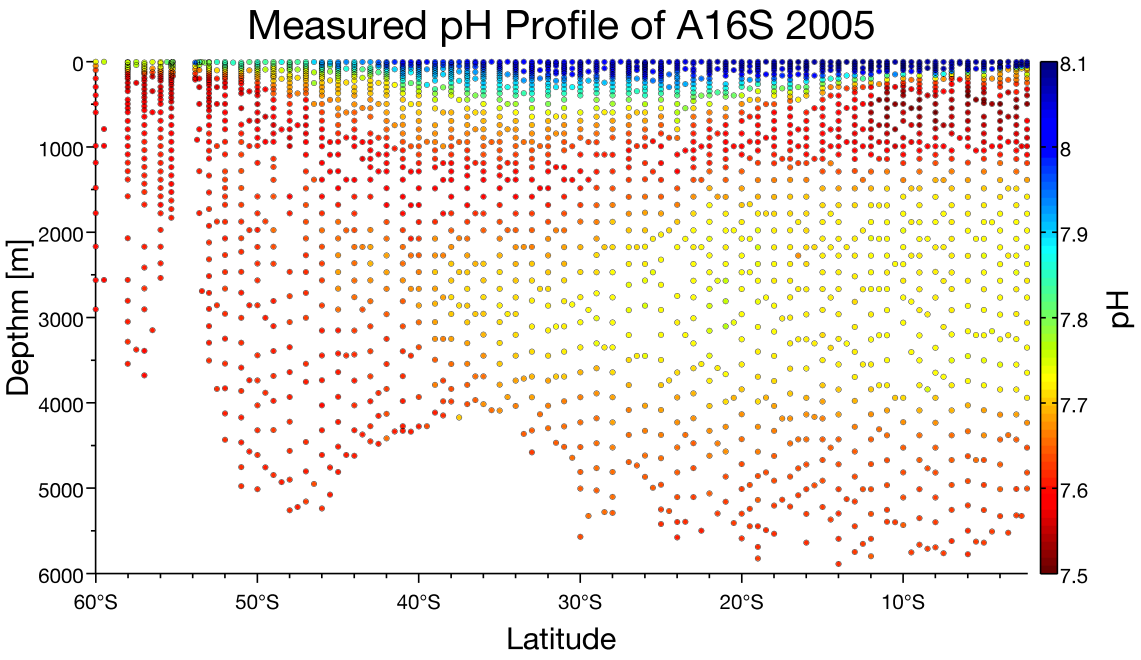

Figure 2.5: A profile of Measured pH values along the A16S transect, which was occupied in 2005. NADW can be seen in this plot as the higher pH values coming from the north, AAIW can be seen as the lower pH water above NADW along with SAMW above AAIW, and AABW can be seen under the NADW. UCDW and LCDW are harder to define based on pH values, but they would be located south of NADW where the three water masses mix together (Figure 1.9).

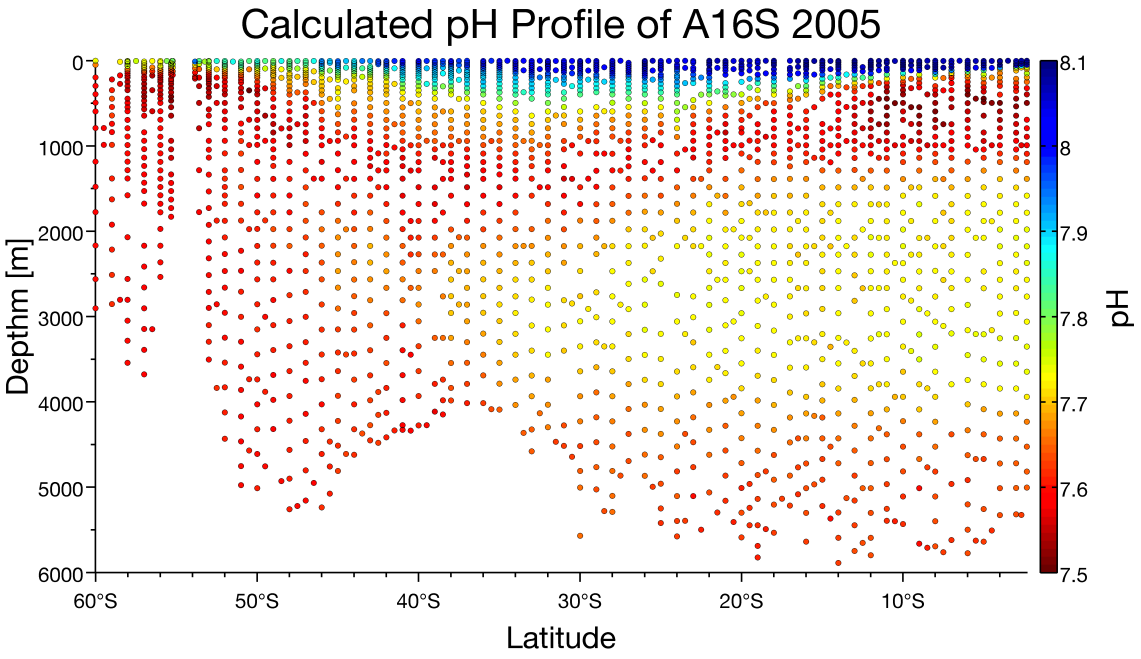

Figure 2.6: A profile of Calculated pH values along the A16S transect, which was occupied in 2005, demonstrates the potential for calculating pH and creating an array of pH data through the Southern Ocean where pH was not measured.

Chapter 3

Calculating pH in the Southern Ocean and Determining Change

3.1 Introduction

In order to calculate pH in the Southern Ocean, the optimized pH calculations discussed in Section 2.4 were used to calculate the most accurate pH values where no pH measurements previously existed. Calculations throughout the Southern Ocean were performed using the Millero et al. (2006) carbonic acid dissociation constants to calculate pH values on the seawater scale at 25°C. These calculated pH values were used to investigate pH changes along the repeat hydrographic transects throughout the Southern Ocean to identify trends throughout the water column and in regions where further investigations should be focused. Three transects, one in each of the major ocean basins (Atlantic, Indian and Pacific), were further investigated to determine the significance of the changes in pH that were observed. As a result of our calculations, we were able to more than double the southern hemisphere pH coverage, which increased the temporal coverage by approximately 20 years. The calculated pH values were also used to determine significant pH changes throughout the top 1 km of the water column.

3.2 Improving the Southern Ocean pH Dataset

Using all of the cruise data that spans back to 1972 with the Atlantic GEOSECS cruise, there were only 20 cruises that measured pH, with the first being in 1992 and the most recent being 2011

(Figure 3.1a). Considering this, the measured Southern Ocean pH dataset has large gaps in the Pacific region where no data exists north of 65°S between 110°W to 170°W and the eastern edge of the Pacific also lacks pH measurements. There is only one cruise between these two large areas, which would otherwise leave the South Pacific Ocean without any pH measurements north of 65°S with the P15S transect in the Southwest Pacific as the only exception. Another gap is in the Indian Ocean where virtually no pH measurements have been taken with a few sparse exceptions. There are also no pH measurements in the Atlantic region south of 60°S.

Now, if we consider pH in the Southern Ocean using the 20 cruises that measured pH and an additional 47 cruises that measured the other inorganic carbon parameters that we used to calculate pH, the Southern Ocean pH coverage improves dramatically (Figure 3.1b). As a result of these calculated pH values, the gaps in the Pacific region previously described are filled, along with the Indian region, which now has extensive spatial pH data coverage. The Atlantic region has also

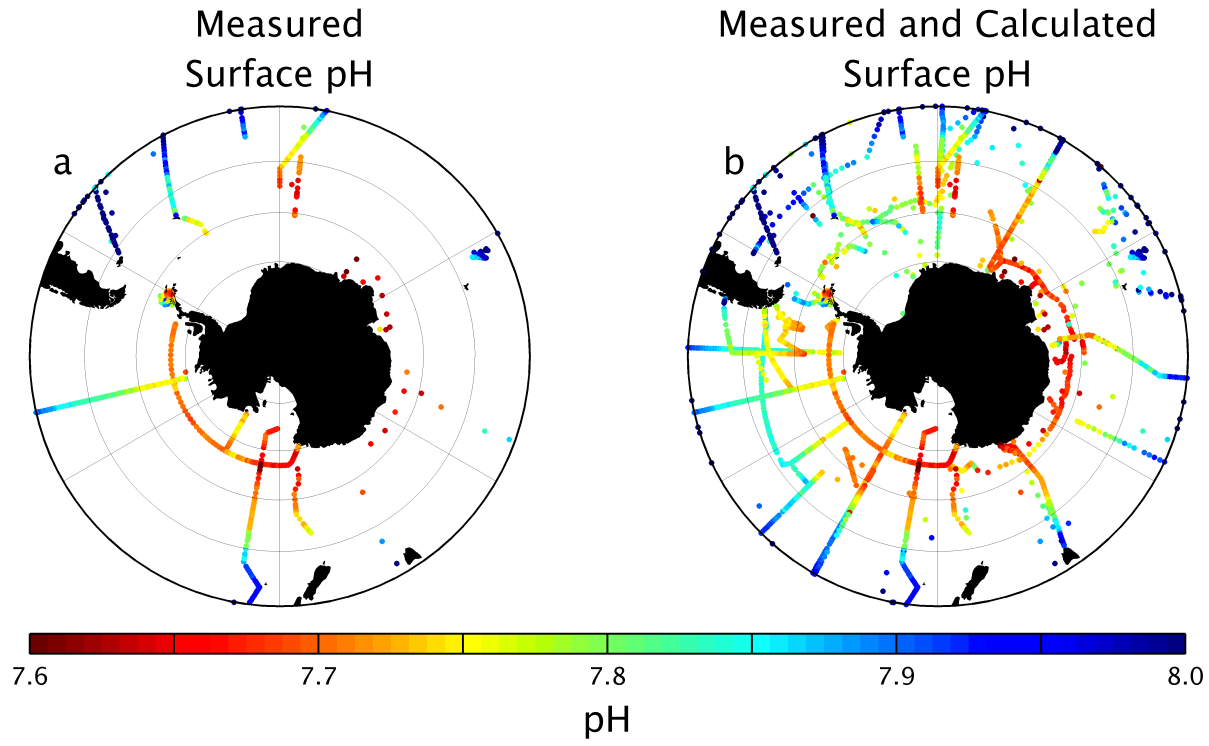

Figure 3.1: Comparison of (a) only measured pH and (b) measured and calculated pH in the top 30 m of the Southern Ocean. The decreasing poleward pH trend is due to the trend in temperature, and the increased dissociation of CO_3^{2-} at lower temperatures. The pH decreases as more CO_3^{2-} dissociates, which dissociates more readily in the colder waters at higher latitudes. All pH values are on the seawater scale at 25°C.

been improved with pH data south of 60°S, with some data even extending into the Weddell Sea. The majority of this coverage is due to calculated pH values from the WOCE era in the 1990s, and many of those transects were repeated through CLIVAR in the 2000s so there is a substantial amount of pH overlap for determining change along repeat transects. There were some additional cruises, primarily in the Atlantic and Indian regions, that took place during the 1980s, not to mention the three GEOSECS cruises in each of the three major ocean basins during the 1970s. Using CO2SYS to calculate pH throughout the Southern Ocean as discussed in Section 2.4, we more than doubled the pH data and substantially improved the pH coverage of the Southern Ocean.

3.3 Binning pH Location for Decadal Comparison

In order to compare pH from two different occupations of the same transect, a couple of adjustments had to be made to the locations of pH values from the intial and final transect occupations so we could determine decadal change. We accomplished this by binning pH data locations and by normalizing the time between measurements to one decade, assuming the change was linear. The majority of the transects were meridional (Figure 3.1b), especially when considering transects that were repeated, and when the transects were repeated the longitude was more or less consistent with the previous occupation. This was also true with zonal transects when repeated, i.e., latitude was consistent for both occupations, but since zonal cruises were less common and less frequently repeated we will refer to the meridional cruises to explain our binning method.

Considering the repeated meridional cruises, there was little variation in the longitude of the sampling locations between occupations, however, there were variations in the depths and latitudes that samples were collected at (Figure 3.2a). In order for us to determine pH change, i.e., subtract the final pH value from the initial pH value, we had to bin the sampling locations so they overlapped. This was accomplished by binning the latitude by 0.5° in the top 1 km of the water column, and by 1° below the top 1 km of the water column. We used a similar technique for depth with slightly more variation, which is summarized in Table 3.1 and the result of binning in situ data can be seen in Figure 3.2b.

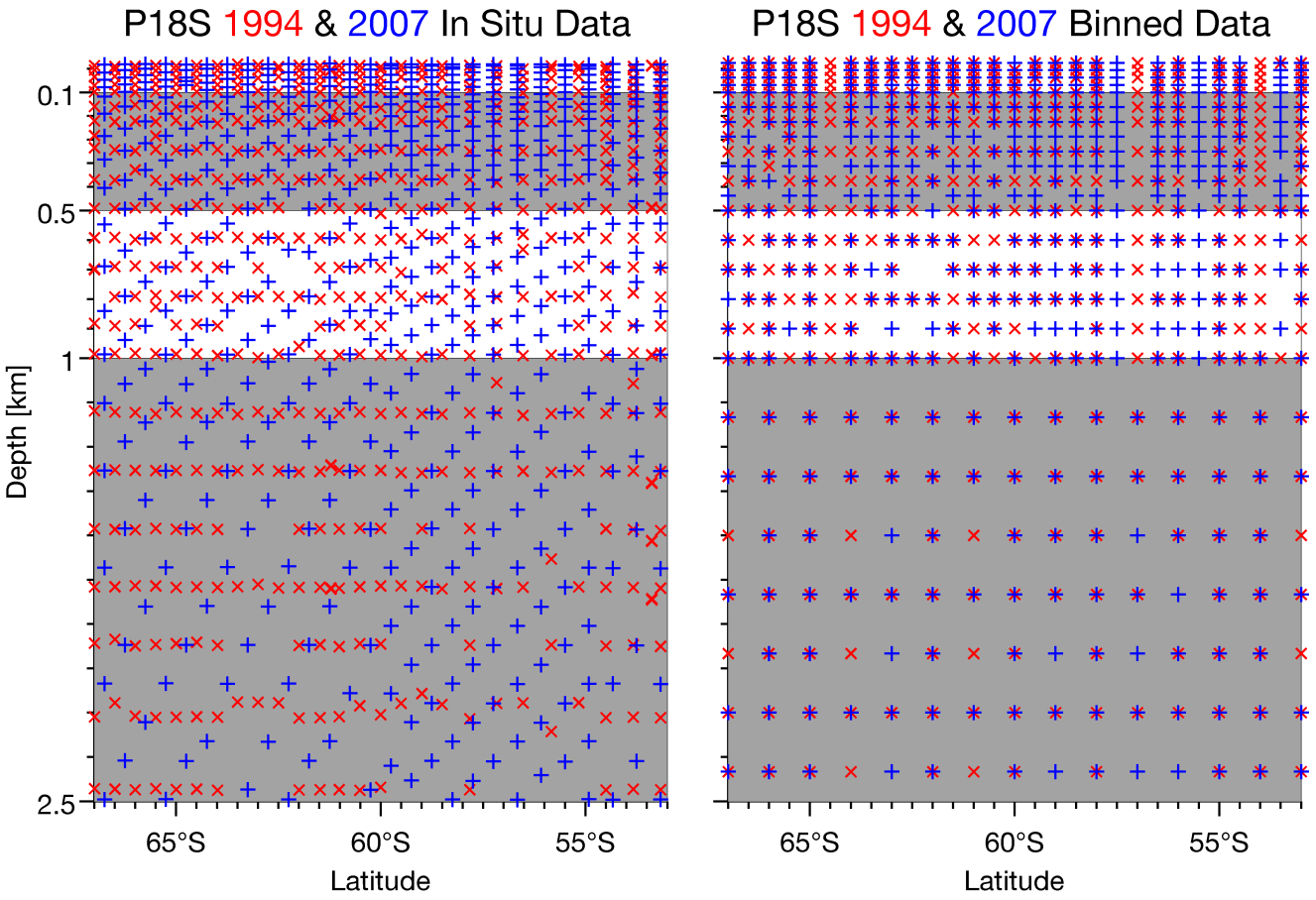

Figure 3.2: Comparison of in situ (a) and binned (b) data locations from both occupations of the P18S transect in the South Pacific.

In order to normalize the time interval between cruises to one decade, we converted the measurement date (in YYYYMMDD format) to Julian days, and divided by 365.25 days per year (0.25 to account for leap years) to determine the measurement dates in decimal years (DY), or mathematically:

$$\mathrm{DY} = \frac{\text{Julian days}}{365.25 \text{ days year}^{-1}}. \tag{3.1}$$

Measurement dates were converted to decimal years for the initial (DY_i) and final (DY_f) transect occupations and the difference between pH values from the initial (pH_i) and final (pH_f) occupations were divided by the change in decimal years (ΔDY) and multiplied by ten years to determine the decadal pH change ($\Delta\mathrm{pH}_{10}$), or mathematically:

$$\Delta\mathrm{pH}_{10} = \frac{\Delta\mathrm{pH}}{\Delta\mathrm{DY}} \cdot 10 \text{ years} = \frac{\mathrm{pH}_f - \mathrm{pH}_i}{\mathrm{DY}_f - \mathrm{DY}_i} \cdot 10 \text{ years}. \tag{3.2}$$

Depth Binning Scheme for pH Comparison	
Depth Bin Range (m)	Bin Size (m)
<100	25
100-500	50
500-1000	100
>1000	200

Table 3.1: Depth binning scheme for pH comparison. This scheme was used for a majority of the cruises for pH comparison, however, pH overlap was not maximize using this scheme for some repeated cruises and the binning scheme was slightly altered (A16S and SR02).

These calculations normalized the time elapsed between pH values to be one decade, with the assumption that pH change (ΔpH) was linear. If multiple pH values existed in the same bin, the mean of the pH values was taken before determining the change in pH. Once pH change was determined, multiple profile plots of decadal pH change were made for the various transects that were repeated to determine the cruises that should be further investigated to determine significant pH change. The profile plots were produced with a program called Easy Krig 3.0 (Chu, 2004), which was used to interpolate pH change throughout space to obtain a more clear understanding of decadal pH change (Figures 3.3-3.4 and A.1-A.4).

Based on the decadal pH change profiles that were produced, we decided to focus our attention on three transects, one in each major ocean basin with the A16S transect representing the Atlantic, the I08S transect representing the Indian, and the P18S transect representing the Pacific regions of the Southern Ocean (Figure 3.3). The depth binning scheme for these three transects was consistent, but latitude bins for A16S were 1° in the top 1 km of the ocean, as opposed to 0.5°. The SR02 transect from Antarctica to the Cape of Good Hope brought the limitations of our method to our attention by eddies from the Agulhas Current having pH signatures associated with them (Figure 3.4). Because of this limitation, and the realization that there may be discrepancies in our comparison method due to the dynamics of the surface ocean, we decided to look at pH change within the bins as opposed to interpolated pH changes. Additional decadal pH change profiles can be found in the Appendix in Section A.1.

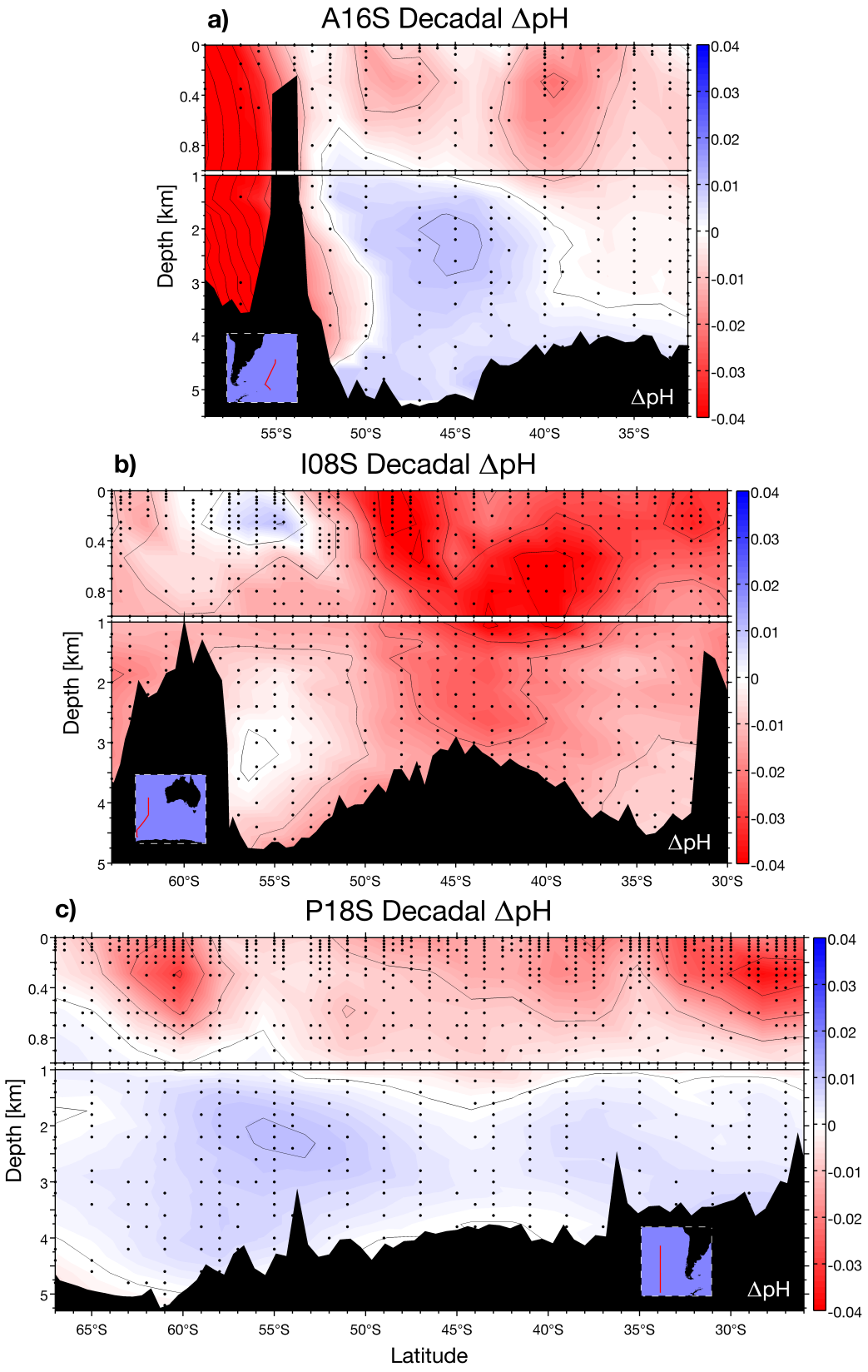

Figure 3.3: Interpolated decadal pH change along (a) A16S in the South Atlantic, (b) I08S in the eastern Indian Ocean, and (c) P18S in the southeastern Pacific Ocean. Contours represent 0.01 ΔpH.

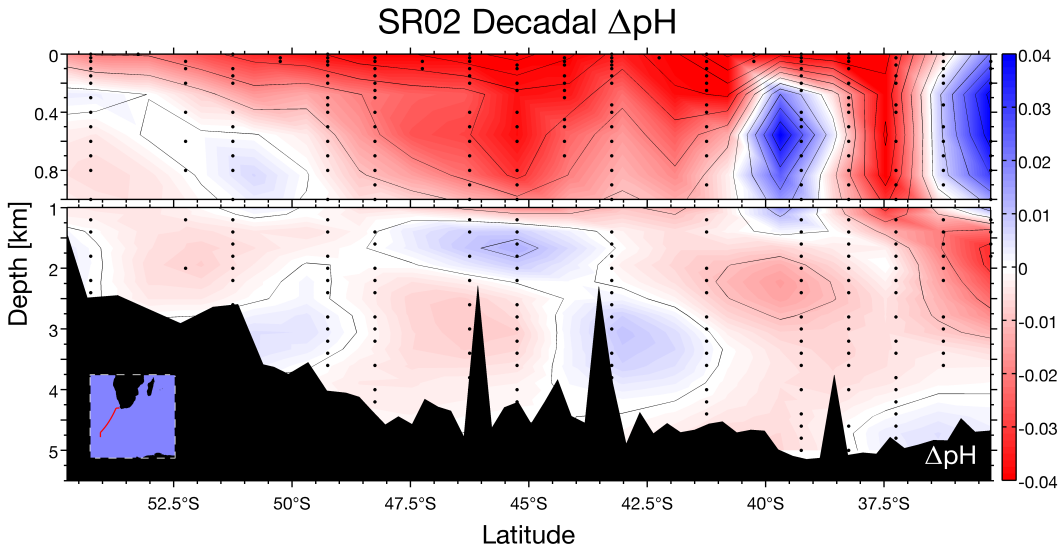

Figure 3.4: Decadal pH change along the SR02 transect in the southeastern Atlantic Ocean using data from the SR02 transects. Contours represent 0.01 ΔpH. Note: the same binning scheme used for A16S was used for SR02.

3.4 Binned pH Change

Since assumptions in the location of the pH values were made with the binning of the data in order to determine pH change, we were interested to plot what the pH values filling the binned areas looked like. We understood that by interpolating pH values over areas where no pH was present, we made other assumptions that smoothed over those areas, possibly inaccurately representing pH change where no data existed. We were interested to investigate our binning method to determine change where we could, and not plot any pH values in the bins where no pH change was determined. These plots not only display pH data in a way spatially consistent with our binning methods (Section 3.3), but the bins themselves display pH change over a majority of the profiles and sufficiently map decadal pH change throughout the water column (Figure 3.5).

Due to a majority of the bins being close to white ($\Delta pH = 0$), especially below 1 km, we decided that we should consider the associated pH error that was determined in Section 2.3. This was done by eliminating pH change if the associated pH error, propagated from both pH values used to determine pH change, was larger than the pH change itself (Section 3.5).

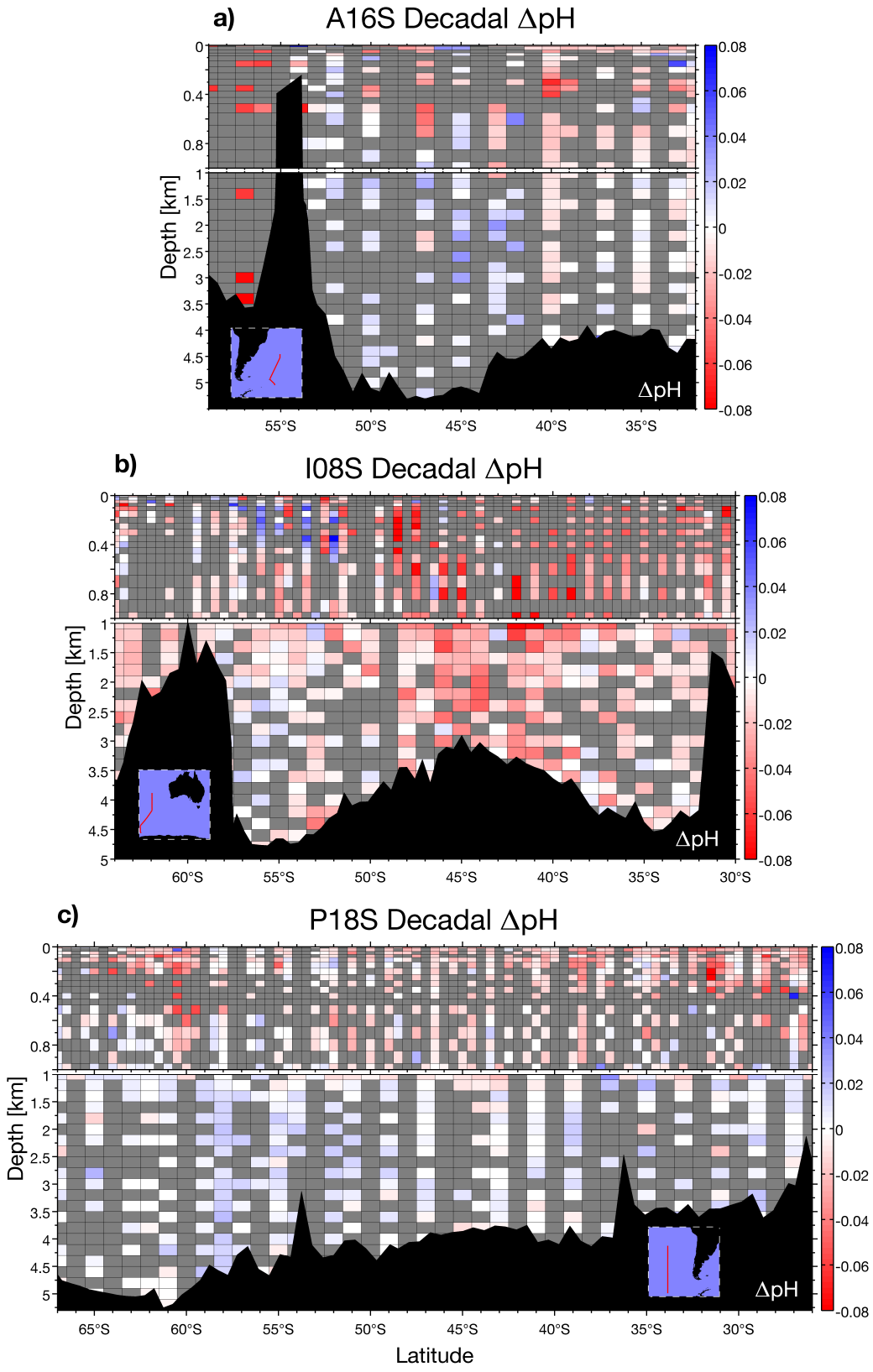

Figure 3.5: Binned decadal pH change along (a) A16S in the South Atlantic, (b) I08S in the eastern Indian Ocean, and (c) P18S in the southeastern Pacific Ocean (c). To be compared with interpolated pH change in Figure 3.3 (note the different color bar scale).

3.5 Error Propagation and Significant pH Changes

Since the error associated with pH measurements and calculations was in some cases larger than the pH change itself, we decided to propagate error from the two pH values used to determine ΔpH in order to compare propagated error with ΔpH. The error propagation performed to determine the error associated with ΔpH was performed in the same manor as propagating the precision estimates from bottle samples and the pH_{calc} accuracy estimate to determine the overall pH_{calc} error (eq. 2.7). The propagated error associated with ΔpH ($\sigma_{\Delta\mathrm{pH}}$) was calculated based on the following equation:

$$\sigma_{\Delta\mathrm{pH}} = \sqrt{(\sigma_{calc}(\mathrm{pH}_f))^2 + (\sigma_{calc}(\mathrm{pH}_i))^2}, \tag{3.3}$$

where $\sigma_{calc}(\mathrm{pH}_f)$ is the error associated with pH_{calc} from the final occupation, and $\sigma_{calc}(\mathrm{pH}_i)$ is the error associated with pH_{calc} from the initial occupation.

If multiple pH values existed in the same bin, we used the pH value with the smallest associated error, which in some cases was measured pH values. The error for pH_{meas} was also determined in a similar manor to pH_{calc} (eq. 2.7), however, rather than using σ_{calc}, we used the accuracy estimate of pH_{meas} (σ_{acc}) determined for the corresponding cruise, and for this determination, eq. 2.7 became

$$\sigma(\mathrm{pH}_{meas}) = \sqrt{(\frac{1}{n}\sum_{i=0}^{n}\sigma_{rep})^2 + {\sigma_{acc}}^2} \tag{3.4}$$

for measured pH error. If a pH accuracy estimate was not reported for the corresponding cruise, the accuracy of the pH measurement was determined by using the Dickson's Certified Reference Material (CRM) used during the cruise (Dickson, 2001). Since CRM's are only produced for DIC and TA, the CRM values were converted into a relative error and multiplied by the mean of pH_{rep} measurements to determine the measured pH error (σ_{meas}) as follows:

$$\sigma_{meas} = \sqrt{{\overline{\sigma}_{rep}}^2 + (\frac{\sigma_{\mathrm{CRM}} \cdot \overline{\mathrm{pH}}_{rep}}{\mathrm{CRM}})^2}, \tag{3.5}$$

where σ_{CRM} is the reported error of the CRM measurement (for either DIC or TA), and CRM is the reported CRM value (for either DIC or TA, respectively). The bar denotes the mean of repeat

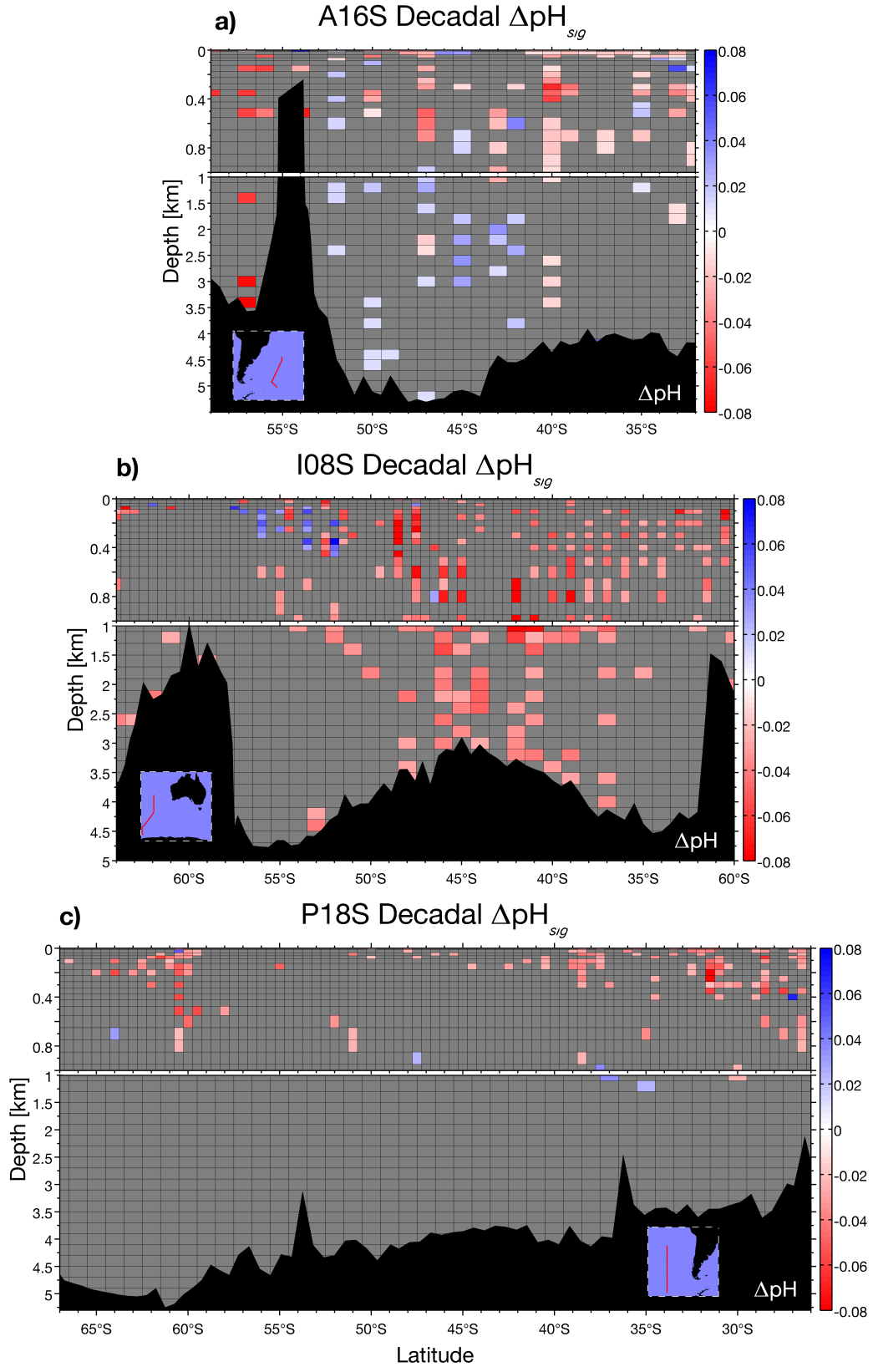

Figure 3.6: Binned significant decadal pH change along (a) A16S in the South Atlantic, (b) I08S in the eastern Indian Ocean, and (c) P18S in the southeastern Pacific Ocean. To be compared with binned pH change (Figures 3.5).

measurements. A general expression for the determination of $\sigma_{\Delta\text{pH}}$ using either calculated and/or measured pH values is

$$\sigma_{\Delta\text{pH}} = \sqrt{{\sigma_f}^2 + {\sigma_i}^2}, \tag{3.6}$$

where σ_f is the error from the final pH value and σ_i is the error from the initial pH value.

Once the error was propagated for ΔpH, the binned errors were used to determine significant pH change (ΔpH_{sig}), i.e., the ΔpH larger than the propagated error, which is represented as bins in profiles of ΔpH_{sig} (Figure 3.6). In order to determine ΔpH_{sig}, we did not simply subtract the propagated error from ΔpH (or add if ΔpH was negative). We treated ΔpH differently depending on two conditions. If ΔpH was larger than the associated error we did not alter ΔpH value because ΔpH was more significant than the propagated error. If ΔpH was smaller than the associated error, ΔpH was masked so ΔpH was not displayed in the corresponding bin. Overall, the significant decadal pH change in the top 1 km was determined to be -0.02 ± 0.03 for the A16S profile, -0.04 ± 0.04 for the I08S profile, -0.04 ± 0.03 for the P18S profile, and the average decadal pH change for all three transects was determined to be -0.03 ± 0.03.

Since there is so much variability in the surface ocean, it is hard to distinguish between trends in pH and sort-term changes such as the pH changes caused by the Agulhas current as represented in Figure 3.4. However, the overall pH change throughout the Southern Ocean of -0.03 ± 0.03 suggests that the surface ocean pH has changed, and is decreasing. This decadal change of -0.03 also matches the estimated -0.3 decrease in surface ocean pH predicted to occur by the end of the century determined by Orr et al. (2005) and Brewer (1997) using the 'busines-as-usual' CO_2 emissions scenario. In order to further investigate short-term changes in the surface ocean that could lead to changes in pH, we compared changes in pH with respect to changes in isopycnal surfaces.

3.6 Changes with Respect to Isopycnal Surfaces

It was mentioned in Section 3.3, that changes in pH in the top 1 km of the ocean can be caused by eddies, such as in Figure 3.4 with the Agulhas Current, and this limitation of dynamic changes

in pH in the upper ocean was brought to our attention. It has been mentioned that changes in pH due to eddies that either upwell DIC-rich water, which lowers the pH, or downwell water that is not in equilibrium with the atmosphere, which could raise or lower the pH depending on the pCO_2 content of that water. Biological activity does not change the TA of the water by very much, but it does change the DIC content, which in turn changes the pH (Figure 1.3). Photosynthesis performed by phytoplankton during their blooms consumes DIC, which increases the pH (Figure 1.3). Conversely, after the plankton favorable season ends, the phytoplankton die and settle throughout the water column as POC, and this decay or respiration releases DIC and the pH increases (Figure 1.3). Additionally, when TA is held constant, which is not always the case for this process, the dissolution of CO_3^{2-} lowers pH and the precipitation of CO_3^{2-} increases the pH (Figure 1.3).

Because of these natural changes in the carbon chemistry throughout the water column, there will be seasonal changes in pH in the upper ocean caused by changes in circulation, biological activity, and temperature. Since the repeat cruises do not always sample during the same month as the initial cruise, it's possible that some the pH change that we are observing is due to these short-lived processes rather than due to climatic changes. In order for us to address this issue, we considered changes in pH with respect to changes in isopycnal surfaces to determine areas where changes in density, possibly due to seasonal changes or circulation variations, could be influencing pH. Density was calculated from measured salinity, temperature and pressure using the equation of state (Fofnoff, 1985), and was plotted over ΔpH in the top 1 km of the water column as contour lines in order to compare any correlations between the two different changes (Figure 3.7). We investigated these possibly related changes along the A16S, I08S and P18S transects (Figure 3.7). We limited the depth to a maximum of 1 km for our comparison of pH change with respect to isopycnal changes because density did not change much at depths greater than 1 km and we also considered the months of the initial and final occupations (Table 3.2). These transects will be discussed in the order of their appearance in Figure 3.7, however, the focus will be on the Indian region of the Southern Ocean because of the spatial coverage of the pH data points and the interesting isopycnal features.

Southern and Northernmost Sampling Dates						
	Southernmost Sampling Dates			Northernmost Sampling Dates		
Transect	Final	Initial	ΔMonths	Final	Initial	ΔMonths
A16S (N. of 54°S)	1/20	2/17	∼1	2/03	2/01	∼0
A16S (S. of 54°S)	1/17	4/08	∼3	1/20	4/12	∼3
I08S	2/18	12/28	∼2	3/12	12/5	∼3
P18S	2/16	2/27	∼1	1/16	3/23	∼2

Table 3.2: The sampling dates of the southernmost and northernmost points of the transects in each of the major ocean basins. Note the ∼3 month differences in the southern portion of A16S and in the northern portion of I08S.

In the Atlantic region of the Southern Ocean (Figure 3.7a), there is a large decrease in pH between 50°S and 35°S that crosses the 27 potential density surface, which is not what we would expect because mixing normally takes place along isopycnal surfaces rather than across them. There is also another decrease in pH south of 55°S that crosses the 27.5 isopycnal, again, not what we would expect. Both of these changes are likely due to the poor spatial coverage, however, the southern most pH decrease could be due to the three month difference in sampling (Table 3.2). If we consider changes in the isopycnal surfaces we might be able to resolve these unexpected diapycnal changes, but because the spatial coverage is so poor, it is hard to draw any conclusions from this profile.

In the Indian region of the Southern Ocean (Figure 3.7b), changes in pH seem to be following along isopycnals as we would expect. The increase in pH along the 27.5 isopycnal appears to be correlated with decreased density at both the 27 and 27.5 isopycnal surfaces between 57°S and 50°S, which would be characterized by the downward flow of water. This process could raise the pH by the water at the surface not being in equilibrium with the atmospheric CO_2 concentration before descending, which would raise the pH. If this were the case, this increase in pH would be associated with a cyclonic eddy, which could also explain the increase in pH north of 35°S in Figure 3.7a. In addition to the density change in Figure 3.7b between 57°S and 50°S, density increases around 40°S, which would be characterized by the upward flow of DIC-rich water, and could in turn lower the pH. Since the decrease in pH along the 27 isopycnal in Figure 3.7b is for the most part not associated with changes in density, this could be evidence for how the Indian

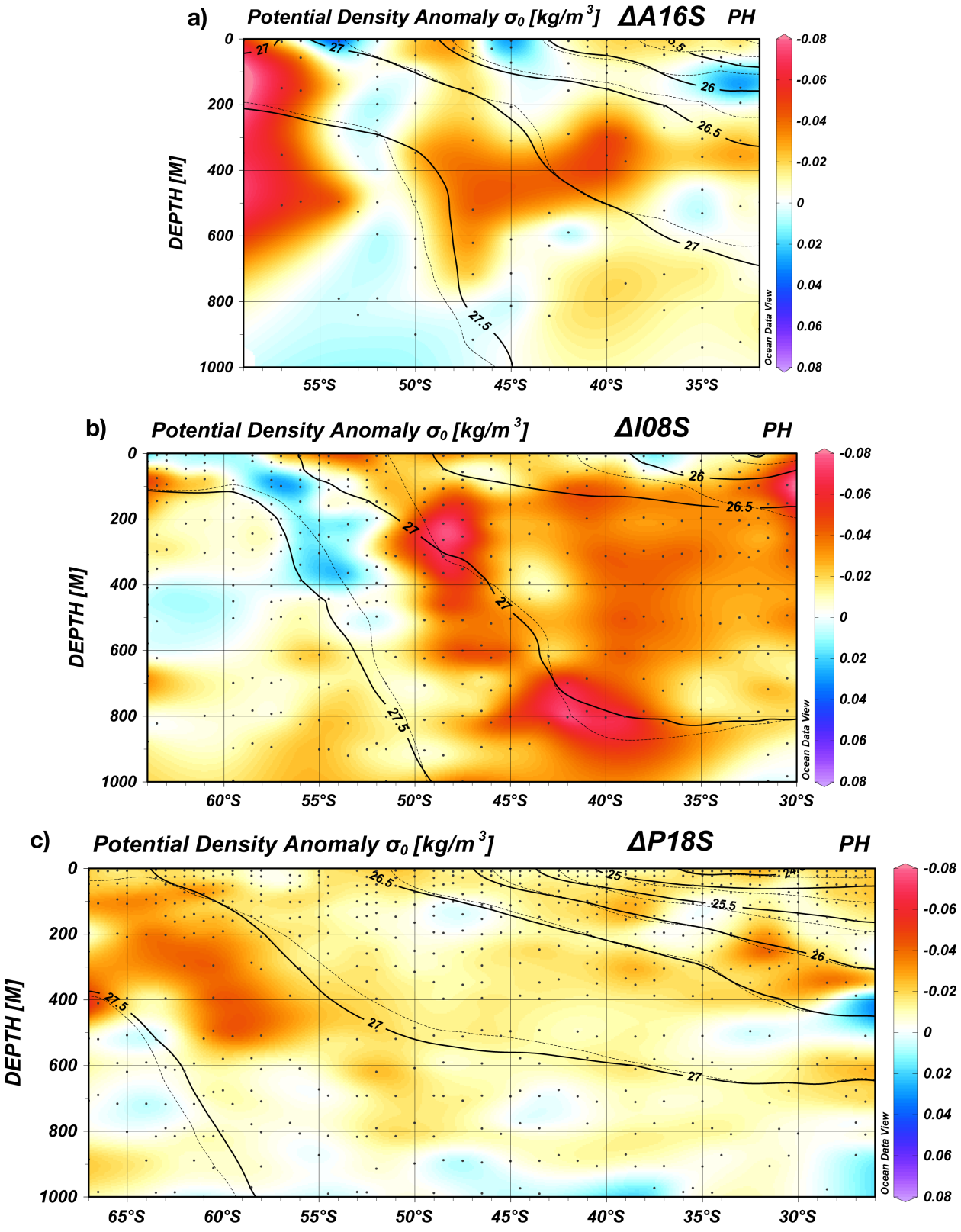

Figure 3.7: Decadal pH change with respect to isopycnal changes along the (a) A16S, (b) I08S, and (c) P18S transects. Colors represent pH change and contours represent isopycnal surfaces. Dashed contours represent the isopycnal surfaces during the initial occupation while solid contours represent the isopycnal surfaces during the final occupation.

Ocean's chemistry is changing due to climate, rather than weather or seasonal changes. The overall decrease in pH above the 27 isopycnal could also be due to the strong SAMW influence in the Indian Ocean, or it could be due to the three month difference in sampling (Table 3.2).

In the Pacific Ocean (Figure 3.7c) the pH change does not appear to be as strong when compared to the Atlantic or Indian Ocean, but there also does not seem to be significant changes in isopycnals, which could be the cause of many of these observed changes. There does seem to be a fairly strong decrease between the 27 and 27.5 isopycnal surfaces, or roughly along the 27.25 isopycnal. This decrease in pH could be due to the formation of AAIW and the subduction of CO_2 rich waters, which would lower the pH along an isopycnal surface as expected.

3.7 Results and Discussion

Through this study, we have determined that significant pH changes have occurred in the top 1 km of the ocean in all three major ocean basins in the southern hemisphere, and this significant pH change is fairly consistent throughout the top 1 km as a decrease in pH (Figure 3.6). Some areas in the top 1 km do not have a consistent decrease in pH as we would have expected (Figure 3.4), which is likely due to seasonal or short-lived changes such as eddies upwelling or downwelling water in the top 1 km. To address this issue, contour plots of isopycnal surfaces during the initial and final occupations were plotted on top of pH change to determine how pH was changing with respect to density (Figure 3.7). This approach was successful in identifying areas where pH change could be associated with seasonal or short-lived changes rather than climatological changes. We also considered the sampling months of each transect occupation, and noticed that if the month of the initial sampling was three months away from the month of the final cruise sampling, there were larger changes in pH, which could be due to the difference in the months when samples were collected.

Through our analysis of decadal pH change along repeat hydrographic transects, we have determined that the pH in the surface ocean has on average decreased. This pH decrease in the top 1 km is significant, and has decreased by -0.03 ± 0.03 pH over the course of one decade. The decadal decrease in pH of -0.03 throughout the top 1 km of the Southern Ocean that we

determined is consistent with the estimated -0.3 decrease in surface ocean pH predicted to occur by the end of the century if surface ocean pH is decreasing linearly over time (Orr et al., 2005; Brewer, 1997). For the most part, changes in pH observed below 1 km were insignificant, which is due to small changes in pH at depth as opposed to larger measurement or calculation errors when compared to pH changes determined in the top 1 km. There was significant decrease in pH below 1 km in the Indian Ocean, which could be due to deeper SAMW in the Indian Ocean. However, since we did not see this trend throughout all of the ocean basins in the southern hemisphere, it is hard to draw conclusions from this without speculation.

Chapter 4

Summary and Conclusions

The pH data calculated from this study were used to determine decadal pH change throughout the southern hemisphere, primarily focusing on three repeat transects; the A16S transect in the South Atlantic Ocean, the I08S transect in the Indian Ocean, and the P18S in the South Pacific Ocean (Figures 3.3, 3.5-3.7). We determined the decadal pH change along other transects, although, we did not determine if these changes were significant compared with their associated error (Figures 3.4, A.1-A.4). Because of the variations in the top 1 km of the water column as represented in Figure 3.4, we decided to compare decadal changes in pH with respect to isopycnal changes between the initial and final measurements (Figure 3.7). Through this analysis we concluded that some changes in pH could be attributed to seasonal and short-lived changes such as eddies, and that discerning pH changes caused by the dynamics of the surface ocean is possible, however, it is challenging when considering changes in density that might influence changes in pH.

Since pH can be influenced by dynamic changes in density, caused eddies and similar features in the ocean, we feel that it would be important to reevalute these pH changes using density as the y coordinate rather than depth. By doing this we feel that many of the unexpected pH changes would disappear, and that the overall evaluation would be improved. We also feel that comparing decadal pH changes with respect to changes in isopycnal surfaces, similar to Figure 3.7, would be useful for transects like SR02 that collected samples from within eddies (Figure 3.4), which would improve our understanding of how eddies and similar features can temporarily influence pH. We are also interested in looking at the significance of decadal pH change for other transects that were repeated to determine if the changes that we are observing are indeed significant.

Finally, we feel that it would be interesting to determine trends in pH that extend back to the 1970s, utilizing the GEOSECS data. This would be performed to determine pH trends more broadly throughout the Southern Ocean by calculating regressions over time. Also, limiting the determination of these pH trends to the three regions of the Southern Ocean (Atlantic, Indian, and Pacific) and zonally could prove to be useful in understanding how the Southern Ocean's pH has been changing since the 1970s. In order to determine these trends effectively, the location of pH will be defined by density rather than depth in order to minimize the impacts that surface ocean dynamics have on pH.

As a result of calculating pH to determine pH changes throughout the Southern Ocean, we were able to increase the number of pH data points with our calculated pH values. By utilizing the CO2SYS program, we were able to produce pH data for 47 cruises that did not measure pH, which increased the temporal coverage of pH in the Southern Ocean by approximately 20 years (Figure 4.1). Measured pH values in the Southern Ocean prior to our study spanned from 1992 to 2011 and after our calculations pH values exist throughout the Southern Ocean spanning from 1972 to 2011, doubling the temporal pH coverage (Figure 4.1). Initially there were just over 31,000 pH measurements in the southern hemisphere, and after our calculations there are now more than 73,000 pH values spanning approximately 40 years (Figure 4.1) and extending to $\sim$78°S (Figures 3.1b and 4.2). Prior to this study, only 17,614 pH measurements existed south of 30°S, and only 5,416 south of 60°S. As a result of this study, there are now more than 52,407 pH values that exist south of 30°S (34,793 being calculated) and 15,074 south of 60°S (9,658 being calculated) – nearly tripling the Southern Ocean and Antarctic pH datasets.

The overall conclusions from this study were that the best carbonic dissociation constants to use for the CO2SYS calculation are the Millero et al. (2006) dissociation constants, and that pH has significantly changed in the top 1 km throughout the Southern Ocean, with pH decreasing by -0.03 ± 0.03 pH units over the course of one decade (Figure 3.6).

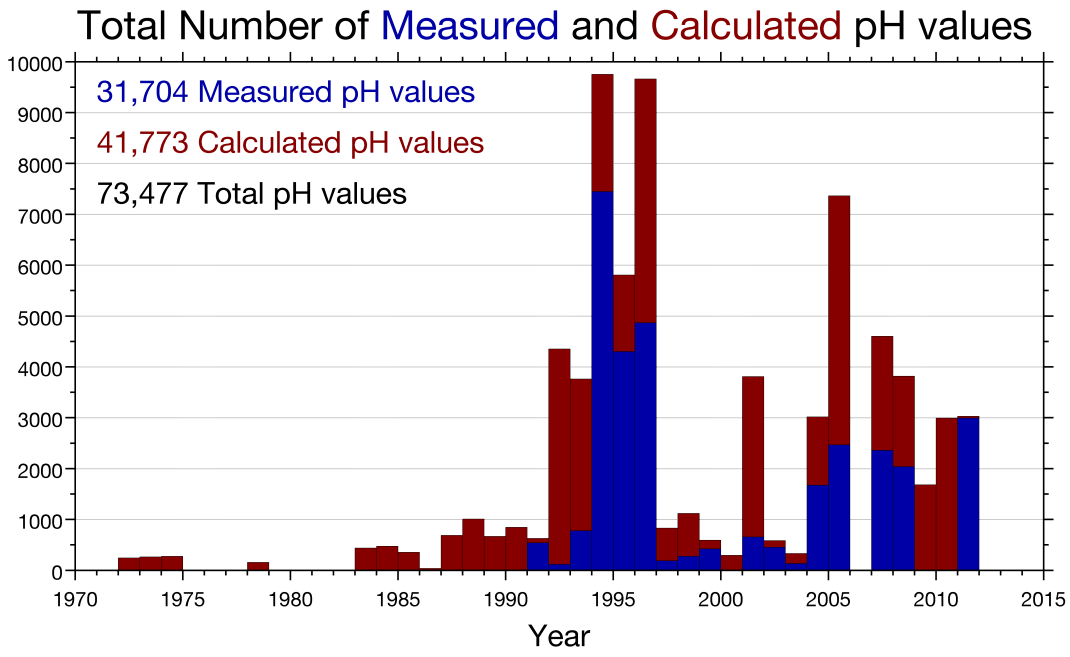

Figure 4.1: The total number of southern hemisphere pH values as a result of this study with respect to year. Blue bars symbolize measured pH values and red bars symbolize calculated pH values with a grand total of 73,477 pH values throughout the southern hemisphere.

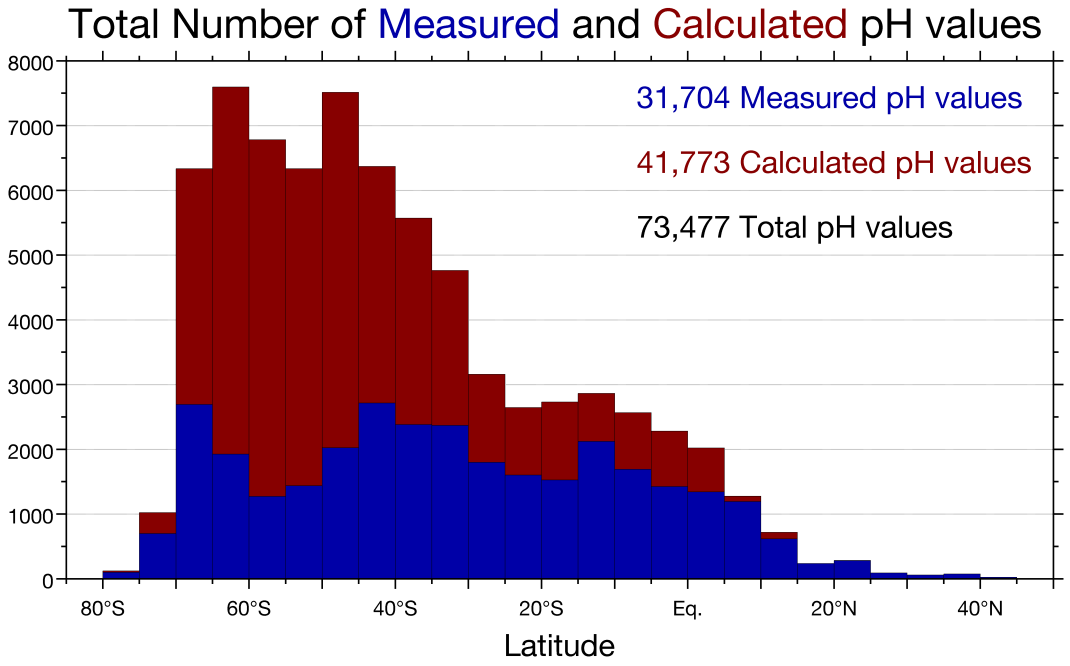

Figure 4.2: The total number of southern hemisphere pH values as a result of this study with respect to latitude. Blue bars symbolize measured pH values and red bars symbolize calculated pH values with a grand total of 73,477 pH values throughout the southern hemisphere.

Appendix A

Figures

A.1 Profiles of Decadal pH Change

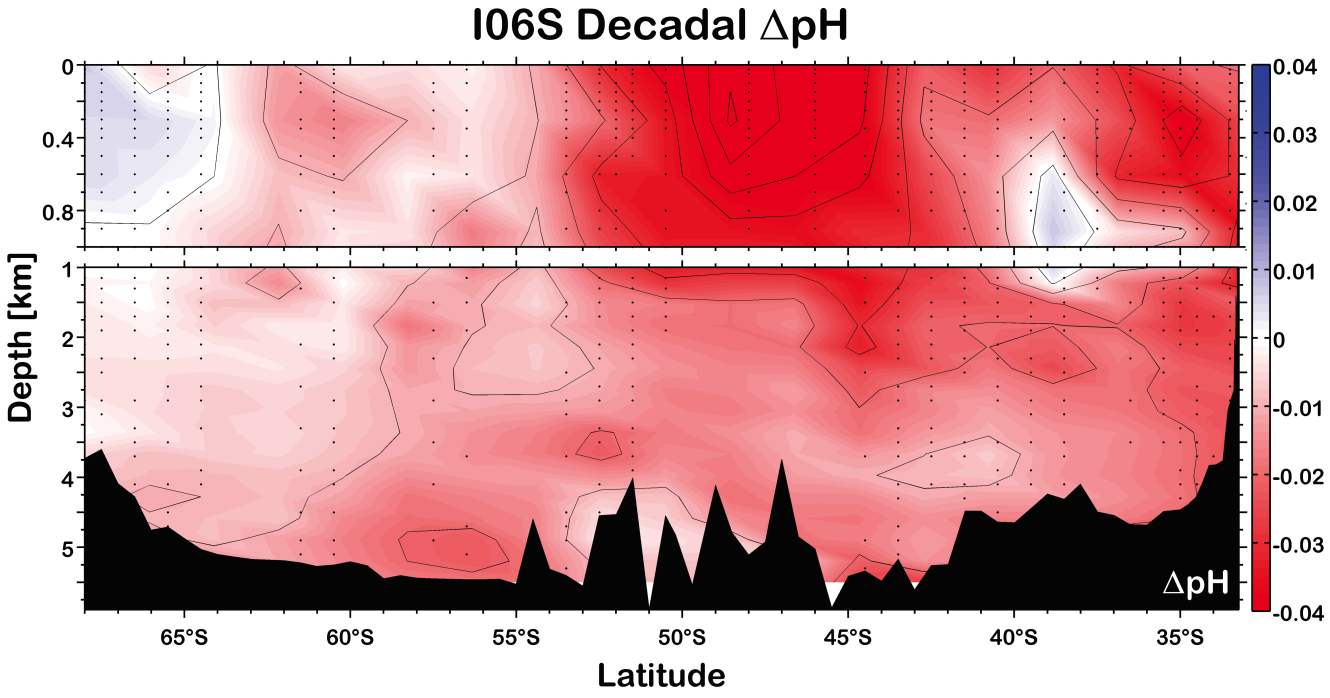

Figure A.1: Decadal pH change along the meridional I06S transect in the southwestern Indian Ocean. Contours represent 0.01 ΔpH. Note: The binning scheme used to produce this plot is slightly different than the one described in Table 3.1.

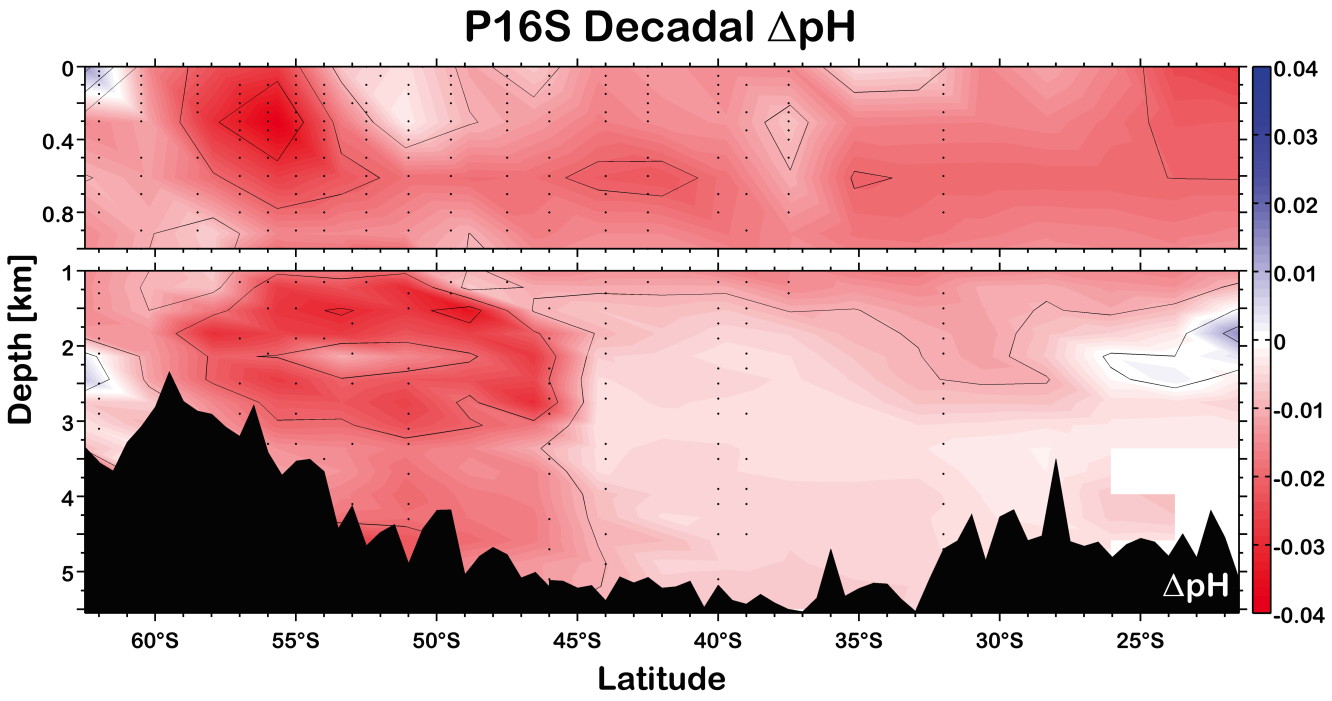

Figure A.2: Decadal pH change along the meridional P16S transect in the southwestern Pacific Ocean. Contours represent 0.01 ΔpH. Note: The binning scheme used to produce this plot is slightly different than the one described in Table 3.1.

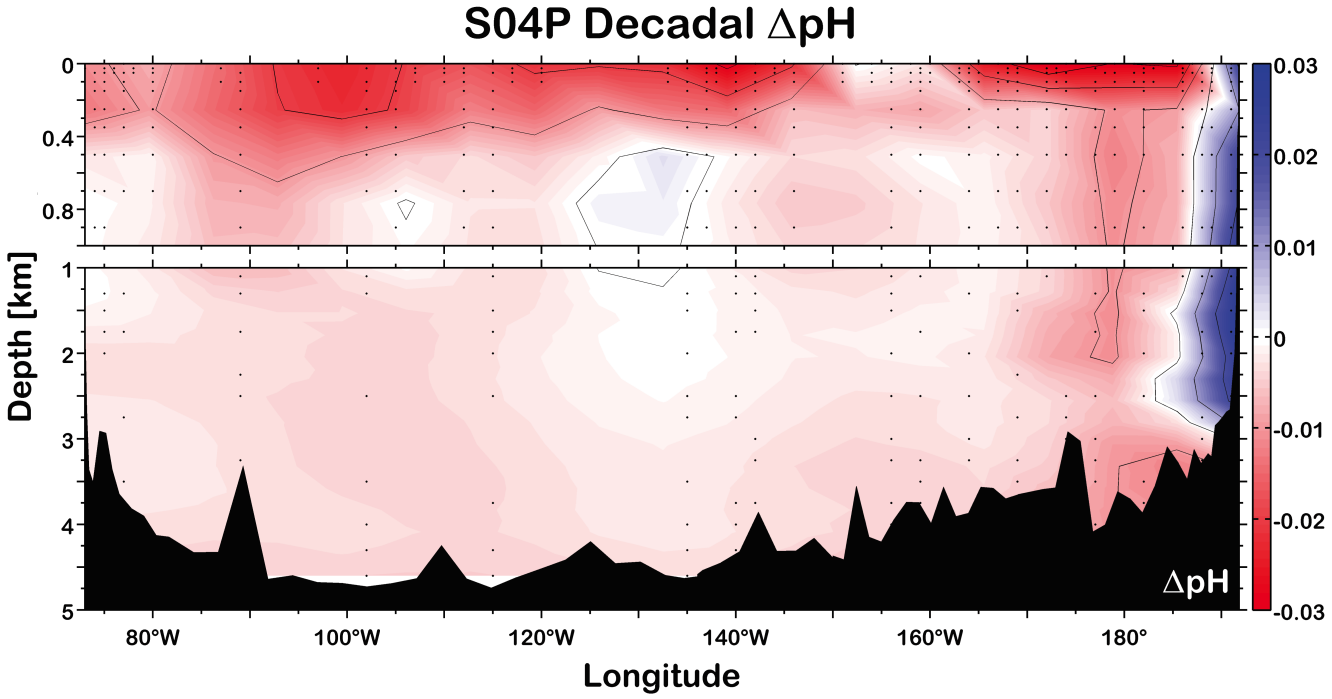

Figure A.3: Decadal pH change along the zonal S04P transect across the South Pacific region of the Southern Ocean. Contours represent 0.01 ΔpH. Note: The binning scheme used to produce this plot is slightly different than the one described in Table 3.1.

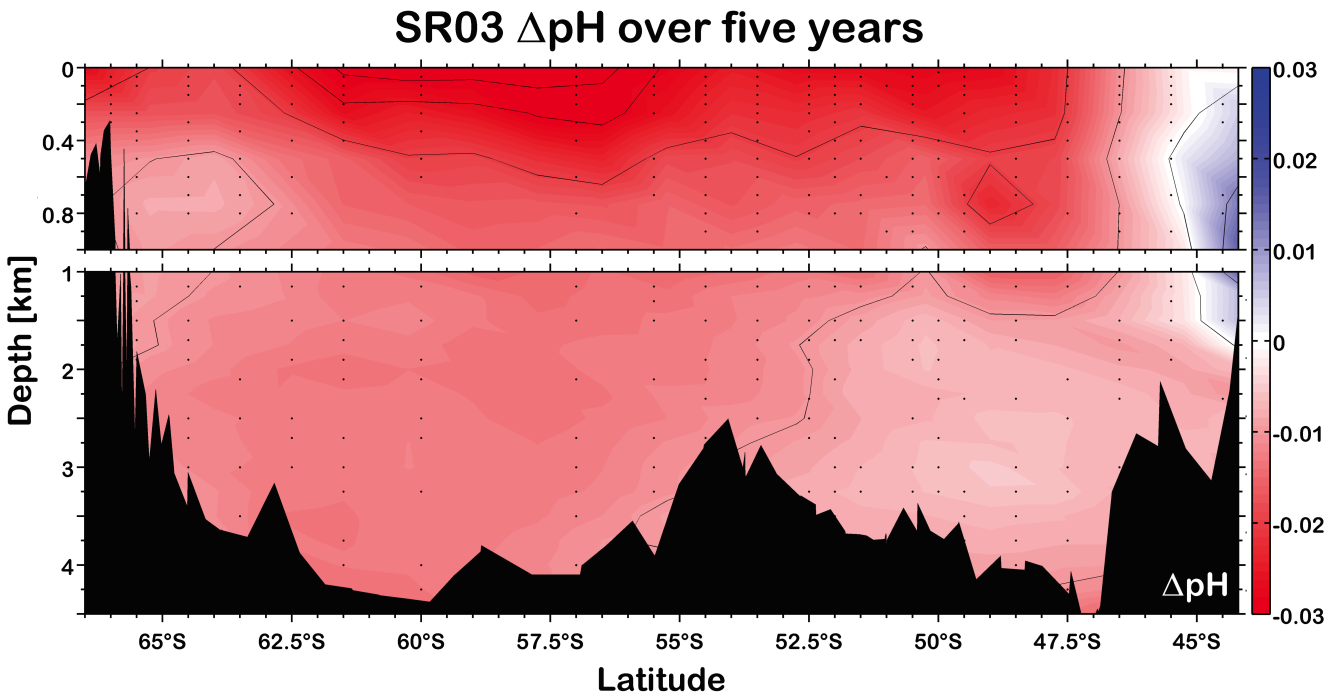

Figure A.4: Five-year pH change along the meridional SR03 transect between Antarctica and Tazmania. Contours represent 0.01 ΔpH. Note: The binning scheme used to produce this plot is slightly different than the one described in Table 3.1.

Appendix B

Tables

B.1 CO2SYS pH_{calc} RMSE for Carbonic Acid Dissociation Constants

Note: Dissociation constants were abbreviated for the tables by the number used in CO2SYS, and the dissociation constants are numbered as follows:

1 Roy et al. (1993)

2 Goyet and Poisson (1989)

3 Hansson (1973b,a) refit by Dickson and Millero (1987)

4 Mehrbach et al. (1973) refit by Dickson and Millero (1987)

5 Hansson (1973b,a) and Mehrbach et al. (1973) refit by Dickson and Millero (1987)

6 GEOSECS (Takahashi et al., 1982)

9 Millero et al. (2006)

10 Lueker et al. (2000)

Cruises that Measured DIC and TA and the Associated pH_{calc} RMSE									
Dissociation Constants		1	2	3	4	5	6	9	10
Cruise	Year	RMSE	RMSE	RMSE	RMSE	RMSE	RMSE	RMSE	RMSE
75°N	1995	0.0240	0.0218	0.0222	0.0247	0.0227	0.0326	0.0276	0.0291
75°N	1998	0.0113	0.0151	0.0234	0.0295	0.0248	0.0416	0.0345	0.0367
A05	1992	0.0336	0.0316	0.0315	0.0335	0.0318	0.0396	0.0357	0.0370
A10	2003	0.0319	0.0254	0.0164	0.0118	0.0152	0.0105	0.0090	0.0083
A13.5	2010	0.0312	0.0250	0.0164	0.0144	0.0182	0.0082	0.0102	0.0082
A14*	1995	0.1197	0.1135	0.1075	0.1048	0.1099	0.0942	0.1009	0.0967
A16N	1993	0.0149	0.0103	0.0098	0.0119	0.0091	0.0203	0.0157	0.0183
A16N	2003	0.0273	0.0217	0.0155	0.0137	0.0148	0.0200	0.0146	0.0157
A16S Leg 1*	1991	0.0946	0.1006	0.1094	0.1120	0.1075	0.1198	0.1168	0.1197
A16S	2005	0.0362	0.0299	0.0215	0.0173	0.0205	0.0129	0.0142	0.0131
A17	1994	0.0122	0.0143	0.0183	0.0203	0.0165	0.0305	0.0237	0.0273
A20	1997	0.0313	0.0245	0.0151	0.0094	0.0137	0.0096	0.0064	0.0062
A22	1997	0.0260	0.0192	0.0101	0.0057	0.0087	0.0138	0.0067	0.0084
AOS	1996	0.0175	0.0175	0.0218	0.0261	0.0227	0.0366	0.0302	0.0323
AOS	2005	0.0516	0.0464	0.0416	0.0406	0.0436	0.0354	0.0377	0.0350
AR01	1998	0.0224	0.0161	0.0092	0.0088	0.0085	0.0183	0.0120	0.0139
FICARAM	2003	0.0351	0.0285	0.0196	0.0141	0.0182	0.0109	0.0111	0.0102
I0304	2003	0.0342	0.0277	0.0188	0.0146	0.0178	0.0102	0.0110	0.0095
I05	2002	0.0239	0.0191	0.0150	0.0152	0.0148	0.0261	0.0172	0.0186
I05	2009	0.0299	0.0239	0.0158	0.0135	0.0173	0.0122	0.0107	0.0100
Line P Leg 1	2010	0.0227	0.0185	0.0158	0.0167	0.0159	0.0265	0.0177	0.0189
Line P Leg 2	2010	0.0222	0.0176	0.0138	0.0136	0.0136	0.0245	0.0144	0.0157
ORI-855	2008	0.0251	0.0191	0.0126	0.0134	0.0123	0.0216	0.0164	0.0178
P01	1999	0.0381	0.0354	0.0344	0.0362	0.0350	0.0382	0.0359	0.0355
P01	2007	0.0321	0.0260	0.0188	0.0178	0.0194	0.0094	0.0137	0.0107
P02T*	1994	0.1006	0.0977	0.0947	0.0943	0.0947	0.0896	0.0929	0.0919
P06	2003	0.0343	0.0279	0.0194	0.0155	0.0185	0.0111	0.0122	0.0108
P06W	2009	0.0336	0.0273	0.0190	0.0145	0.0178	0.0156	0.0121	0.0117
P06	2010	0.0334	0.0273	0.0189	0.0141	0.0177	0.0163	0.0115	0.0112
P10	2005	0.0259	0.0198	0.0126	0.0111	0.0123	0.0178	0.0099	0.0099
P14 Leg 1	2007	0.0323	0.0262	0.0189	0.0175	0.0188	0.0112	0.0138	0.0112
P14 Leg 2	2007	0.0298	0.0233	0.0146	0.0107	0.0137	0.0121	0.0073	0.0062
P14N	1993	0.0243	0.0213	0.0202	0.0213	0.0203	0.0330	0.0233	0.0247
P14S	1996	0.0187	0.0129	0.0077	0.0086	0.0074	0.0250	0.0124	0.0147
P1415S	1996	0.0109	0.0082	0.0120	0.0163	0.0129	0.0342	0.0212	0.0237
P16N	2006	0.0199	0.0183	0.0189	0.0190	0.0186	0.0363	0.0223	0.0248
P17N	2001	0.0420	0.0364	0.0299	0.0293	0.0300	0.0172	0.0259	0.0232
P18	2007	0.0267	0.0214	0.0156	0.0139	0.0151	0.0223	0.0141	0.0151
P21EW	1994	0.0433	0.0399	0.0365	0.0357	0.0363	0.0378	0.0353	0.0353
P21 Leg 1	2009	0.0393	0.0325	0.0230	0.0176	0.0218	0.0048	0.0126	0.0102
P21 Leg 2	2009	0.0414	0.0349	0.0265	0.0228	0.0257	0.0062	0.0180	0.0152
S04P	2011	0.0378	0.0320	0.0249	0.0220	0.0243	0.0180	0.0192	0.0180
SR04	1997	0.0280	0.0313	0.0377	0.0419	0.0387	0.0509	0.0461	0.0482

Table B.1: Calculated pH values using DIC and TA from forty-three different cruises. *Values were excluded from the CO2SYS accuracy determination based on questionable data determined by Dixon's Q-test at the 95% confidence level (Rorabacher, 1991). For dissociation constant number assignment, see note at beginning of Section B.1.

Cruises that Measured TA and pCO_2 and the Associated pH_{calc} RMSE									
Dissociation Constants		1	2	3	4	5	6	9	10
Cruise	Year	RMSE	RMSE	RMSE	RMSE	RMSE	RMSE	RMSE	RMSE
A13.5	2010	0.0081	0.0101	0.0113	0.0101	0.0091	0.0084	0.0079	0.0083
A16N	1993	0.0138	0.0184	0.0206	0.0083	0.0163	0.0163	0.0120	0.0165
A16N	2003	0.0133	0.0144	0.0156	0.0135	0.0151	0.0169	0.0135	0.0149
A16S Leg 1*	1991	0.1228	0.1276	0.1297	0.1161	0.1254	0.1250	0.1206	0.1253
A16S	2005	0.0080	0.0084	0.0097	0.0091	0.0091	0.0105	0.0077	0.0088
A20	1997	0.0052	0.0047	0.0065	0.0065	0.0057	0.0073	0.0038	0.0055
A22	1997	0.0066	0.0060	0.0074	0.0079	0.0068	0.0082	0.0056	0.0067
A24	1997	0.0179	0.0230	0.0256	0.0156	0.0248	0.0266	0.0204	0.0244
AR01	1998	0.0096	0.0132	0.0155	0.0080	0.0146	0.0174	0.0110	0.0145
FICARAM*	2003	0.0410	0.0391	0.0381	0.0414	0.0385	0.0379	0.0395	0.0382
P14S	1996	0.0075	0.0057	0.0065	0.0100	0.0062	0.0074	0.0069	0.0062
P1415S	1996	0.0073	0.0116	0.0138	0.0063	0.0129	0.0153	0.0091	0.0126
P16N	2006	0.0128	0.0165	0.0181	0.0107	0.0170	0.0206	0.0132	0.0166
P18	2007	0.0099	0.0095	0.0102	0.0115	0.0099	0.0118	0.0097	0.0098

Table B.2: Calculated pH values using TA and pCO_2 from fourteen different cruises. *Values were excluded from the CO2SYS accuracy determination based on questionable data determined by Dixon's Q-test at the 95% confidence level (Rorabacher, 1991). For dissociation constant number assignment, see note at beginning of Section B.1.

Cruises that Measured DIC and pCO_2 and the Associated pH_{calc} RMSE									
Dissociation Constants		1	2	3	4	5	6	9	10
Cruise	Year	RMSE	RMSE	RMSE	RMSE	RMSE	RMSE	RMSE	RMSE
A13.5	2010	0.0090	0.0118	0.0128	0.0101	0.0097	0.0088	0.0082	0.0089
A16N	1993	0.0158	0.0204	0.0220	0.0084	0.0174	0.0161	0.0119	0.0164
A16N	2003	0.0139	0.0156	0.0166	0.0140	0.0160	0.0170	0.0139	0.0153
A16S Leg 1*	1991	0.1252	0.1299	0.1313	0.1164	0.1268	0.1254	0.1209	0.1257
A16S	2005	0.0079	0.0097	0.0109	0.0091	0.0101	0.0106	0.0079	0.0092
A20	1997	0.0042	0.0063	0.0080	0.0065	0.0069	0.0074	0.0039	0.0058
A22	1997	0.0060	0.0071	0.0085	0.0083	0.0077	0.0080	0.0059	0.0069
AR01	1998	0.0117	0.0158	0.0177	0.0088	0.0166	0.0181	0.0118	0.0153
FICARAM*	2003	0.0563	0.0570	0.0574	0.0564	0.0574	0.0578	0.0567	0.0571
P14S	1996	0.0074	0.0064	0.0071	0.0111	0.0067	0.0071	0.0078	0.0066
P1415S	1996	0.0084	0.0126	0.0142	0.0066	0.0132	0.0141	0.0086	0.0120
P16N	2006	0.0136	0.0175	0.0187	0.0107	0.0176	0.0200	0.0131	0.0165
P18	2007	0.0110	0.0115	0.0123	0.0128	0.0118	0.0129	0.0112	0.0113

Table B.3: Calculated pH values using DIC and pCO_2 from thirteen different cruises. *Values were excluded from the CO2SYS accuracy determination based on questionable data determined by Dixon's Q-test at the 95% confidence level (Rorabacher, 1991). For dissociation constant number assignment, see note at beginning of Section B.1.

References

Brewer, P., 1997: Ocean chemistry of the fossil fuel CO_2 signal: The haline signal of "business as usual". *Geophysical Research Letters,* **24; 11**, 1367–1369.

Chu, D., 2004: The GLOBEC kriging sofware package: Easy Krig 3.0. http://globec.whoi.edu/software/kriging/easy_krig/easy_krig.html.

Dickson, A., 1981: An exact definition of total alkalinity and a procedure for the estimation of alkalinity and total inorganic carbonfrom titration data. *Deep-Sea Research,* **28A; 6**, 609–623.

Dickson, A., 1990: Standard potential of the reaction: $AgCl_{(s)} + 1/2\ H_{2(g)} = Ag_{(s)} + HCl_{(aq)}$, and the standard acidity constant of the ion HSO_4^- in synthetic seawater from 273.15 to 318.15 K. *Journal of Chemical Thermodynamics,* **22**, 113–127.

Dickson, A., 2001: Reference materials for oceanic CO_2 measurements. *Oceanography,* **14**, 21–22.

Dickson, A. and F. Millero, 1987: A comparison of the equilibrium constants for the dissociation of carbonic acid in seawater media. *Deep-Sea Research,* **34**, 1733–1743.

Doney, S., V. Fabry, R. Feely, and J. Kleypas, 2009: Ocean acidification: The other CO_2 problem. *Annual Review of Marine Science,* **2009.1**, 169–192.

Dore, J., R. Lukas, D. Sadler, M. Church, and D. Karl, 2009: Physical and biogeochemical modulation of ocean acidification in the central North Pacific. *Proceedings of the National Academy of Sciences of the United States of America,* **106**, 12235–12240.

Emerson, S. and J. Hedges, 2008: *Chemical Oceanography and the Marine Carbon Cycle.* New York, New York: Cambridge University Press.

Fabry, V., B. Seibel, R. Feely, and J. Orr, 2008: Impacts of ocean acidification on marine fauna and ecosystem processes. *ICES Journal of Marine Sciences,* **65**, 414–432.

Feely, R., C. Sabine, K.Lee, W. Berelson, J. Kleypas, V. Fabry, and F. Millero, 2004: Impact of anthropogenic CO_2 on the $CaCO_3$ system in the oceans. *Science,* **305**, 362–366.

Fofnoff, N., 1985: Physical properties of seawater: A new salinity scale and equation of state for seawater. *Journal of Geophysical Research,* **90; C2**, 3332–3342.

Goyet, C. and A. Poisson, 1989: New determination of carbonic acid dissociation constants in seawater as a function of temperature and salinity. *Deep-Sea Research,* **36**, 1635–1654.

Gruber, N., P. Friedlingstein, C. Field, R. Valentini, M. Heimann, J. Richey, P. R. Lankao, E.-D. Schulze, and C.-T. Chen, 2004: The vulnerability of the carbon cycle in the 21st century: An assessment of carbon-climate-human interactions. In C. Field and M. Raupach (Eds.), *The Global Carbon Cycle: Integrating Humans, Climate, and the Natural World*, pp. 45–76. Washington, D.C: Island Press.

Hansen, J., M. Sato, R. Ruedy, K. Lo, D. Lea, and M. Medina-Elizade, 2006: Global temperature change. *Proceedings of the National Academy of Sciences,* **103; 39**, 14388–14293.

Hansson, I., 1973a: The determination of dissociation constants of carbonic acid in synthetic sea water in the salinity range of 20 - 40‰ and temperature range of 5 - 30°C. *Acta Chemica Scandanavia,* **27**, 931–944.

Hansson, I., 1973b: A new set of acidity constants for carbonic acid and boric acid in sea water. *Deep-Sea Research,* **20**, 461–478.

Keeling, C., 1960: The concentration and isotpic abundances of carbon dioxide in the atmosphere. *Tellus,* **12**, 200–2003.

Keeling, R., S. Piper, A. Bollenbacher, and S. Walker, 2012: Atmospheric CO_2 concentrations (ppm) derived from in situ air measurements at Mauna Loa, Observatory, Hawaii: Latitude 19.5°N longitude 155.6°W elevation 3397 m. Scripps Institution of Oceanography, La Jolla, California. Scripps CO_2 Program: http://scrippsco2.ucsd.edu.

Klaas, C. and D. Archer, 2002: Association of sinking organic matter with various types of mineral ballast in the deep sea: Implications for the rain ratio. *Global Biogeochemical Cycles,* **16; 4**, 1116–1129.

Kleypas, J., R. Buddemeier, D.Archer, J.-P. Gattuso, C. Langdon, and B. Opdyke, 1999: Geochemical consequences of increased atmospheric carbon dioxide on coral reefs. *Science,* **284**, 118–120.

Kozyr, A., 2011: Ocean CO_2. Carbon Dioxide Information Analysis Center, Oak Ridge National Laboratory, U.S. Department of Energy, Oak Ridge, Tennessee. http://cdiac.esd.ornl.gov/oceans/.

Lüthi, D., M. L. Floch, B. Bereiter, T. Blunier, J.-M. Barnola, U. Siegenthaler, D. Raynaud, J. Jouzel, H. Fischer, K. Kawamura, and T. Stocker, 2008: High-resolution carbon dioxide concentration record $650,000 - 800,000$ years before present. *Nature,* **453**, 379–382.

Lewis, E. and D. Wallace, 1998: *Program Developed for CO_2 System Calculations.* Oak Ridge, Tennessee: Carbon Dioxide Information Analysis Center, Oak Ridge National Laboratory, U.S. Department of Energy. http://cdiac.ornl.gov/oceans/co2rprt.html.

Lovenduski, N. and T. Ito, 2009: The future evolution of the Southern Ocean CO_2 sink. *Journal of Marine Research,* **67**, 597–617.

Lueker, T., A. Dickson, and C. Keeling, 2000: Ocean pCO_2 calculated from dissolved inorganic carbon, alkalinity, and equations for K_1 and K_2: validation based on laboratory measurements of CO_2 in gas and seawater at equilibrium. *Marine Chemistry,* **70**, 105–119.

Mehrbach, C., C. Culberson, J. Hawley, and R. Pytkowicz, 1973: Measurement of the apparent dissociation constants of carbonic acid in seawater at atmospheric pressure. *Limnology and Oceanography,* **18**, 897–907.

Millero, F., 1979: The thermodynamics of the carbonate system in seawater. *Geochemica et Cosmochemica Acta,* **43**, 1651–1661.

Millero, F., 2006: *Chemical Oceanography.* Boca Raton, Florida: CRC Press.

Millero, F., T. Graham, F. Huang, H. Bustos-Serrano, and D. Pierrot, 2006: Dissociation constants of carbonic acid in seawater as a function of salinity and temperature. *Marine Chemistry,* **100**, 80–94.

Murphy, E., J. Watkins, P. Trathan, K. Reid, M. Meredith, S. Thorpe, N. Johnston, A. Clarke, G. Tarling, M. Collins, J. Forcada, R. Shreeve, A. Atkinson, R. Korb, M. Whitehouse, P. Ward, P. Rodhouse, P. Enderlein, A. Hirst, A. Martin, S. Hill, I. Staniland, D. Pond, D. Briggs, N. Cunningham, and A. Fleming, 2007: Spatial and temporal operation of the Scotia Sea ecosystem: a review of large-scale links in a krill centred food web. *Philisophical Transactions of the Royal Society,* **362**, 113–148.

Orr, J., V. Fabry, O. Aumont, L. Bopp, S. Doney, R. Feely, A. Gnanadesikan, N. Gruber, A. Ishida, F. Joos, R. Key, K. Lindsay, E. Maier-Reimer, R. Matear, P. Monfray, A. Mouchet, R. Najjar, G.-K. Plattner, K. Rodgers, C. Sabine, J. Sarmiento, R. Schlitzer, R. Slater, I. Totterdell, M.-F. Weirig, Y. Yamanaka, and A. Yool, 2005: Anthropogenic ocean acidification over the twenty-first century and its impact on calcifying organisms. *Nature,* **437**, 681–686.

Peng, T.-H., T. Takahashi, W. Broecker, and J. Olafsson, 1987: Seasonal variability of carbon dioxide, nutrients and oxygen in the northern North Atlantic surface water: Observations and model. *Tellus,* **39B**, 439–458.

Rorabacher, D., 1991: Statistical treatment for rejection of deviant values: Critical values of Dixons "Q" parameter and related subrange ratios at the 95% confidence level. *Analytical Chemistry,* **63**, 139–146.

Roy, R., L. Roy, K. Vogel, C. Porter-Moore, T. Pearson, C. Good, F. Millero, and D. Campbell, 1993: The dissociation constants of carbonic acid in seawater at salinities 5 to 45 and temperatures 0 to 25°C. *Marine Chemistry,* **44**, 249–267.

Sabine, C., R. Feely, N. Gruber, R. Key, K. Lee, J. Bullister, R. Wanninkhof, C. Wong, D. Wallace, B. Tilbrook, F. Millero, T.-H. Peng, A. Kozyr, T. Ono, and A. Rios, 2004: The oceanic sink for anthropogenic CO_2. *Science,* **305**, 367–371.

Sarmiento, J. and N. Gruber, 2006: *Ocean Biogeochemical Dynamics.* Princeton, New Jersey: Oxford University Press.

Speer, K., S. Rintoul, and B. Sloyan, 2000: The diabatic Deacon cell. *Journal of Physical Oceanography,* **30**, 3212–3222.

Swift, J., S. Diggs, D. Newton, S. Anderson, J. Osborne, and J. Ward, 2001: Improved exchange formate for WHP data. World Ocean Circulation Experiment Hydrographic Program Office, La Jolla, California. http://woce.nodc.noaa.gov/woce_v3/wocedata_1/whp/index.htm.

Swift, J., J. Kappa, and J. Fields, 2012: Clivar and carbon hydrographic data office. La Jolla, California. http://cchdo.ucsd.edu/.

Takahashi, T., S. Sutherland, R. Wanninkhof, C. Sweeney, R. Feely, D. Chipman, B. Hales, G. Friederich, F. Chavez, C. Sabine, A. Watson, D. Bakker, U. Schuster, N. Metzl, H. Yoshikawa-Inoue, M. Ishii, T. Midorikawa, Y. Nojiri, A. Körtzingerm, T. Steinhoffm, M. Hoppema, J. Olafsson, T. Arnarson, B. Tilbrook, T. Johannessen, A. Olsen, R. Bellerby, C. Wong, B. Delille, N. Bates, and H. de Baar, 2009: Climatological mean and decadal change in surface ocean pCO_2 and net sea-air CO_2 flux over the global oceans. *Deep-Sea Research II,* **56**, 554–577.

Takahashi, T., R. Williams, and D. Bos, 1982: Carbonate chemistry. In D. S. W.S. Broecker and H. Craig (Eds.), *GEOSECS Pacific Expedition, Volume 3, Hydrographic Data 1973-1974*, pp. 77–83. Washington, D.C: National Science Foundation.

Talley, L., G. Pickard, W. Emery, and J. Swift, 2011: *Descriptive Physical Oceanography: An Introduction* (sixth ed.). San Diego, California: Elsevier.

Wanninkhof, R. and J. Hendee, 1991: Carbon Dioxide, Hydrographic, and Chemical Data Obtained During the R/V Malcolm Baldrige South Atlantic OACES/CO_2 Cruise, Legs 1 and 2, WOCE Section A16S (11 July - 02 September, 1991). Carbon Dioxide Information Analysis Center, Oak Ridge National Laboratory, U.S. Department of Energy, Oak Ridge, Tennessee. http://cdiac.ornl.gov/ftp/oceans/OACES91_A16S/.

Zachos, J., G. Dickens, and R. Zeebe, 2003: An early cenozoic perspective on greenhouse warming and carbon-cycle dynamics. *Nature,* **451**, 279–283.

Zachos, J., U. Röhl, S. Schellenberg, A. Sluijs, D. Hodell, D. Kelly, E. Thomas, M. Nicolo, I. Raffi, L. Lourens, H. McCarren, and D. Kroon, 2005: Rapid acidification of the ocean during the paleocene-eocene thermal maximum. *Science,* **308**, 1611–1615.

Zeebe, R. and D. Wolf-Gladrow, 2001: *CO_2 in seawater: Equilibrium, kinetics, isotopes.* San Diego, California: Elsevier.